A&A 559, A134 (2013)
DOI: 10.1051/0004-6361/201321993


Astronomy & Astrophysics

# An anisotropic distribution of spin vectors in asteroid families★

J. Hanuš[1], M. Brož[1], J. Ďurech[1], B. D. Warner[2], J. Brinsfield[3], R. Durkee[4], D. Higgins[5], R. A. Koff[6], J. Oey[7], F. Pilcher[8], R. Stephens[9], L. P. Strabla[10], Q. Ulisse[10], and R. Girelli[10]

[1] Astronomical Institute, Faculty of Mathematics and Physics, Charles University in Prague, V Holešovičkách 2, 18000 Prague, Czech Republic
e-mail: hanus.home@gmail.com
[2] Palmer Divide Observatory, 17995 Bakers Farm Rd., Colorado Springs, CO 80908, USA
[3] Via Capote Observatory, Thousand Oaks, CA 91320, USA
[4] Shed of Science Observatory, 5213 Washburn Ave. S, Minneapolis, MN 55410, USA
[5] Hunters Hill Observatory, 7 Mawalan Street, ACT 2913 Ngunnawal, Australia
[6] 980 Antelope Drive West, Bennett, CO 80102, USA
[7] Kingsgrove, NSW, Australia
[8] 4438 Organ Mesa Loop, Las Cruces, NM 88011, USA
[9] Center for Solar System Studies, 9302 Pittsburgh Ave, Suite 105, Rancho Cucamonga, CA 91730, USA
[10] Observatory of Bassano Bresciano, via San Michele 4, Bassano Bresciano (BS), 25020 Brescia, Italy

Received 30 May 2013 / Accepted 16 September 2013

**ABSTRACT**

*Context.* The current number of ~500 asteroid models derived from the disk-integrated photometry by the lightcurve inversion method allows us to study the spin-vector properties of not only the whole population of main-belt asteroids, but also of several individual collisional families.

*Aims.* We create a data set of 152 asteroids that were identified by the hierarchical clustering method (HCM) as members of ten collisional families, among which are 31 newly derived unique models and 24 new models with well-constrained pole-ecliptic latitudes of the spin axes. The remaining models are adopted from the DAMIT database or a few individual publications.

*Methods.* We revised the preliminary family membership identification by the HCM according to several additional criteria: taxonomic type, color, albedo, maximum Yarkovsky semi-major axis drift, and the consistency with the size-frequency distribution of each family, and consequently we remove interlopers. We then present the spin-vector distributions for asteroidal families Flora, Koronis, Eos, Eunomia, Phocaea, Themis, Maria, and Alauda. We use a combined orbital- and spin-evolution model to explain the observed spin-vector properties of objects among collisional families.

*Results.* In general, for studied families we observe similar trends in ($a_p$, $\beta$) space (proper semi-major axis vs. ecliptic latitude of the spin axis): (i) larger asteroids are situated in the proximity of the center of the family; (ii) asteroids with $\beta > 0°$ are usually found to the right of the family center; (iii) on the other hand, asteroids with $\beta < 0°$ to the left of the center; (iv) the majority of asteroids have large pole-ecliptic latitudes ($|\beta| \gtrsim 30°$); and finally (v) some families have a statistically significant excess of asteroids with $\beta > 0°$ or $\beta < 0°$. Our numerical simulation of the long-term evolution of a collisional family is capable of reproducing the observed spin-vector properties well. Using this simulation, we also independently constrain the age of families Flora ($1.0 \pm 0.5$ Gyr) and Koronis (2.5–4 Gyr).

**Key words.** methods: observational – minor planets, asteroids: general – techniques: photometric – methods: numerical

## 1. Introduction

An analysis of rotational state solutions for main belt asteroids has been performed by many authors. All these authors observed the deficiency of poles close to the ecliptic plane (e.g., Magnusson 1986; Drummond et al. 1988; Pravec et al. 2002; Skoglöv & Erikson 2002; Kryszczyńska et al. 2007). Hanuš et al. (2011) showed that this depopulation of spin vectors mainly concerns smaller asteroids ($D \lesssim 40$ km), while the larger asteroids ($60 \lesssim D \lesssim 130$–150 km, Kryszczyńska et al. 2007; Paolicchi & Kryszczyńska 2012) have a statistically significant excess of prograde rotators, but no evident lack of poles close to the ecliptic plane. The observed anisotropy of pole vectors of smaller asteroids is now believed to be a result of YORP thermal torques[1], and of collisions that systematically evolve the spin axes away from the ecliptic plane. The prograde excess of larger asteroids is probably caused by a primordial preference that agrees with the theoretical work of Johansen & Lacerda (2010). While the number of asteroids with known rotational states grows, we can not only study the spin vector distribution in the whole main-belt asteroids (MBAs) or near-Earth asteroids (NEAs) populations, but we can also focus on individual groups of asteroids within these populations, particularly on collisional families (i.e., clusters of asteroids with similar proper orbital elements and often spectra that were formed by catastrophic breakups of parent bodies or cratering events).

★ Tables 3–5 are available in electronic form at http://www.aanda.org

[1] Yarkovsky-O'Keefe-Radzievskii-Paddack effect, a torque caused by the recoil force due to anisotropic thermal emission, which can alter both rotational periods and orientation of spin axes, see e.g., Rubincam (2000).

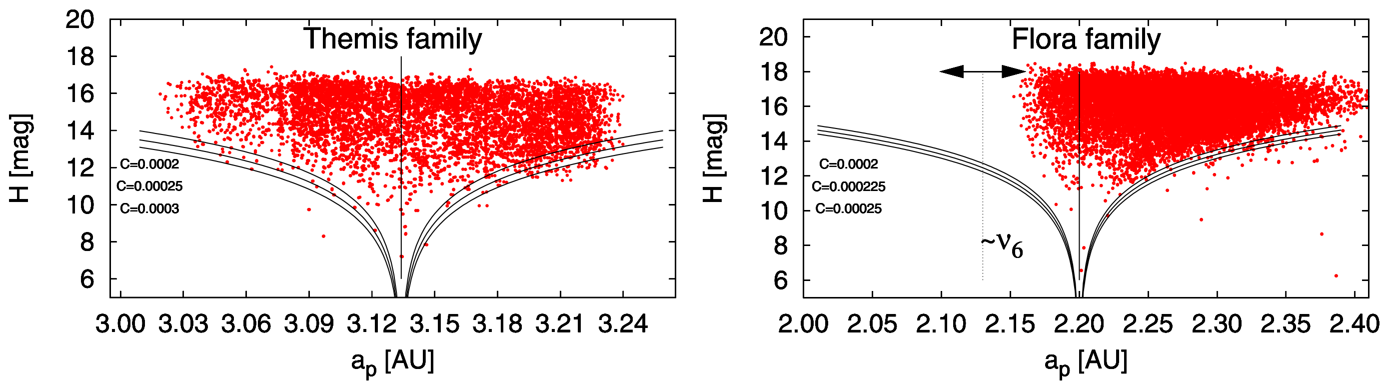


**Fig. 1.** Dependence of the absolute magnitude $H$ on the proper semi-major axis $a_\mathrm{p}$ for the Themis family (*left*) and for the Flora family (*right*) with the likely positions of the family centers (vertical lines). We also plot three ($a_\mathrm{p}$, $H$) borders of the family for different parameters $C$ (different values correspond to a different initial extent of the family or different age and magnitude of the Yarkovsky semi-major axis drift) by gray lines, the optimal border corresponds to the middle line. The vertical dotted line represents the approximate position of the secular $\nu_6$ resonance for the inclination typical for Flora family members and the horizontal arrow its approximate range.

The theory of dynamical evolution of asteroid families (e.g., Bottke et al. 2006) suggests that the Yarkovsky[2]/YORP effects change orbital parameters of smaller asteroids ($\lesssim$30–50 km) – the semi-major axis of prograde rotators slowly grows the course of time, unlike retrograde rotators whose semi-major axis decreases. This phenomenon is particularly visible when we plot the dependence of the absolute magnitude $H$ on the proper semi-major axis $a_\mathrm{p}$ (see an example of such a plot for Themis family in Fig. 1, left panel). In addition, various resonances (e.g., mean-motion resonances with Jupiter or Mars, or secular resonances) can intersect the family and cause a decrease in the number of asteroids in the family by inducing moderate oscillations to their orbital elements (Bottke et al. 2001) as can be seen in Fig. 1 for the Flora family, where the secular $\nu_6$ resonance with Saturn almost completely eliminated objects to the left of the center of the family. The $\nu_6$ resonance has its center at 2.13 AU for objects with $\sin I \sim 0.09$, which is typical of Flora family members. It develops objects which then approach the proximity of the resonance. Some resonances can, for example, capture some asteroids on particular semi-major axes (Nesvorný & Morbidelli 1998).

Laboratory experiments strongly suggest that a collisionally-born cluster should initially have a rotational frequency distribution close to Maxwellian (Giblin et al. 1998) and an isotropic spin vector distribution. For several families, we already know their age estimates (e.g., 2.5 ± 1.0 Gyr for Koronis family, Bottke et al. 2001), and so we have a constraint on the time at which the family was evolving towards its current state. As shown in Bottke et al. (2001), the family evolution is dominated by Yarkovsky and YORP effects, as well as by collisions and spin-orbital resonances. The knowledge of the age should constrain some free parameters in various evolutionary models.

The spin-vector properties in an asteroid family were first studied by Slivan (2002) and Slivan et al. (2003), who reveal an anisotropy of spin vectors for ten members of the Koronis family. This was an unexpected result because collisionallyborn population should have an isotropic spin-vector distribution. The peculiar spin-vector alignment in the Koronis family was explained by Vokrouhlický et al. (2003) as a result of the YORP torques and spin-orbital resonances that modified the spin states over the timespan of 2–3 Gyr. The secular $s_6$ spin-orbital resonance with Saturn may affect the Koronis family members, according to the numerical simulations, it can (i) capture some objects and create a population of prograde rotators with periods $P \in (4, 7)$ h, similar obliquities (42° to 51°) and also with similar ecliptic longitudes in the ranges of (24° to 73°) and (204° to 259°); or (ii) create a group of low-obliquity retrograde rotators with rotational periods $P < 5$ h or $P > 13$ h. The prograde rotators trapped in the $s_6$ spin-orbital resonance were referred to by Vokrouhlický et al. (2003) as being in *Slivan states*. Most members of the Koronis family with known rotational states (determined by the lightcurve inversion by Slivan et al. 2003, 2009; Hanuš et al. 2011, 2013) had the expected properties except for the periods of observed prograde rotators were shifted to higher values of 7–10 h. Rotational states of asteroids that did not match the properties of the two groups were probably reorientated by recent collisions, which are statistically plausible during the family existence for at least a few Koronis members (e.g., asteroid (832) Karin was affected by a collision when a small and young collisional family within the Koronis family was born, Slivan & Molnar 2012).

Another study of rotational states in an asteroid family was made by Kryszczyńska (2013), who focuses on the Flora family. She distinguishes prograde and retrograde groups of asteroids and reports an excess of prograde rotators. This splitting into two groups is most likely caused by the Yarkovsky effect, while the prograde excess by the secular $\nu_6$ resonance that significantly depopulates the retrograde part of the family. See Fig. 1b, only retrograde rotators can drift via the Yarkovsky/YORP effects towards the resonance.

Future studies of rotational properties of collisional families should reveal the influence of the Yarkovsky and YORP effects, and possibly a capture of asteroids in spin-orbital resonances similar to the case of the Koronis family. The Yarkovsky effect should be responsible for spreading the family in a semi-major axis (retrograde rotators drift from their original positions towards the Sun, on the other hand, prograde rotators drift away from the Sun, i.e. towards larger $a_\mathrm{p}$'s), and the YORP effect should eliminate the spin vectors close to the ecliptic plane.

Disk-integrated photometric observations of asteroids contain information about an object's physical parameters, such as the shape, the sidereal rotational period, and the orientation of the spin axis. Photometry acquired at different viewing geometries and apparitions can be used in many cases in a lightcurve inversion method (e.g., Kaasalainen & Torppa 2001; Kaasalainen et al. 2001) and a convex 3D shape model including its rotational

[2] A thermal recoil force affecting rotating asteroids.

state can be derived. This inverse method uses all available photometric data, both the classical dense-in-time lightcurves or the sparse-in-time data from astrometric surveys. Most of the asteroid models derived by this technique are publicly available in the Database of Asteroid Models from Inversion Techniques (DAMIT[3], Ďurech et al. 2010). In February 2013, models of 347 asteroids were included there. About a third of them can be identified as members of various asteroid families. This large number of models of asteroids that belong to asteroid families allows us to investigate the spin-vector properties in at least several families with the largest amount of identified members. Comparison between the observed and synthetic (according to a combined orbital- and spin-evolution model) spin-vector properties could even lead to independent family age estimates.

The paper is organized as follows. In Sect. 2, we investigate the family membership of all asteroids for which we have their models derived by the lightcurve inversion method and present 31 new asteroid models that belong to ten asteroid families. An analysis of spin states within these asteroid families with at least three identified members with known shape models is presented in Sect. 3.1. A combined spin-orbital model for the long-term evolution of a collisional family is described in Sect. 4, where we also compare the synthetic and observed spin-vector properties and constrain the ages of families Flora and Koronis.

## 2. Determination of family members

### 2.1. Methods for family membership determination

For a *preliminary* family membership determination, we adopted an online catalog published by Nesvorný (2012), who used the hierarchical clustering method[4] (HCM, Zappalà et al. 1990, 1994). Nesvorný (2012) used two different types of proper elements for the family membership identification: semi-analytic and synthetic. The more reliable dataset is the one derived from synthetic proper elements, which were computed numerically using a more complete dynamical model. The majority of asteroids are present in both datasets. A few asteroids that are only in one of the datasets are included in the study as well (e.g., asteroids (390) Alma in the Eunomia family or (19848) Yeungchuchiu in the Eos family), because at this stage it is not necessary to remove objects that still could be real family members.

The HCM selects a group of objects that are separated in the proper element space by less than a selected distance. However, not all of these objects are actually real members of the collisionallyborn asteroid family. A fraction of objects have orbital elements similar to typical elements of the asteroid family members only by a coincidence, the so-called interlopers. Interlopers can be identified (and removed), for example, by

- inspection of reflectance spectra. Because they are usually of different taxonomic types those that of the family members, we use the SMASSII (Bus & Binzel 2002) or Tholen taxonomy (Tholen 1984, 1989);
- inspection of colors based on the Sloan Digital Sky Survey Moving Object Catalog 4 (SDSS MOC4, Parker et al. 2008).

[3] http://astro.troja.mff.cuni.cz/projects/asteroids3D

[4] In this method, mutual distances in proper semi-major axis ($a_\mathrm{d}$), proper eccentricity ($e_\mathrm{d}$), and proper inclination ($i_\mathrm{d}$) space are computed. The members of the family are then separated in the proper element space by less than a selected distance (usually, it has a unit of velocity), a free parameter often denoted as "cutoff velocity".

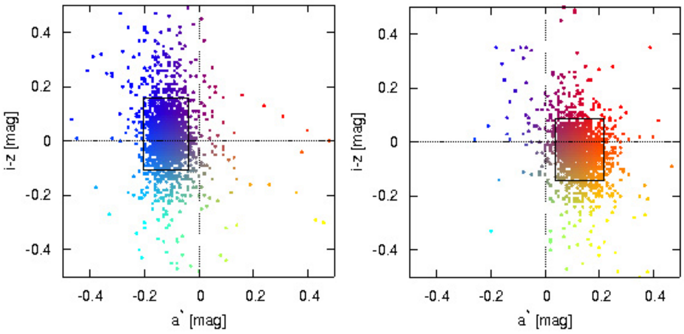


**Fig. 2.** Dependence of the color indexes $a^\star$ and $i-z$ (from the Sloan Digital Sky Survey Moving Object Catalog 4) for a C-type family Themis and S-type family Eunomia. The family corresponds to a compact structure in this parameter space marked by a rectangle. There is a qualitative difference between C- and S-types asteroids.

We used the color indexes $a^\star$ and $i-z$, which usually define the core of the family well (see examples for Themis and Eunomia families in Fig. 2), and for each asteroid with available color indexes, we compared values $a^\star$ and $i-z$ to those that define the family;
- inspection of albedos based on the WISE data (Masiero et al. 2011);
- construction of a diagram of the proper semi-major axis vs. the absolute magnitude (see Fig. 1), estimating the *V-shape* defined by the Yarkovsky semi-major axis drift and excluding outliers, i.e. relatively large asteroids outside the V-shape (see Vokrouhlický et al. 2006b, for the case of the Eos family). We refer here to the ($a_\mathrm{p}$, $H$) border of the family as the border of the V-shape; or by
- construction of a size-frequency distribution (SFD) of the cluster. Some asteroids can be too large to be created within the family and thus are believed to be interlopers (see, e.g., numerical simulations by Michel et al. 2011, who excluded the asteroid (490) Veritas from the Veritas family).

These methods for determining family membership have one common characteristic – we have to determine or choose a range for a quantity that defines the family members (range of spectra, sizes, or distance from the family center), which affects the number of objects we include in the family. Our criteria correspond to the fact that usually 99% of the objects are within the ranges.

### 2.2. New asteroid models

From the DAMIT database, we adopt 96 models of asteroids that are, according to the HCM, members of collisional families. Currently, we have about 100 new asteroid models that have not yet been published. Here, we present new physical models of 31 asteroids from this sample that are identified as members of asteroid families by the HCM. We choose only asteroids that belong to ten specific families for which we expect a reasonable amount of members, i.e., at least three. These convex shape models are derived by the lightcurve inversion method from combined dense and sparse photometry. The derivation process is similar to the one used in Hanuš et al. (2013). The dense photometry was from two main sources: (i) the Uppsala Asteroid Photometric Catalogue (UAPC[5], Lagerkvist et al. 1987; Piironen et al. 2001), where lightcurves for about 1000 asteroids are stored; and (ii) the data from a group of individual observers provided by the Minor Planet Center in the

[5] http://asteroid.astro.helsinki.fi/

**Table 1.** List of new asteroid models derived from combined dense and sparse data or from sparse data alone.

| | Asteroid | $\lambda_1$ [deg] | $\beta_1$ [deg] | $\lambda_2$ [deg] | $\beta_2$ [deg] | $P$ [hours] | $N_{lc}$ | $N_{app}$ | $N_{689}$ | $N_{703}$ | $N_{950}$ |
|---|---|---|---|---|---|---|---|---|---|---|---|
| 243 | Ida | 259 | −66 | 74 | −61 | 4.633632 | 53 | 6 | 134 | 122 | 25 |
| 364 | Isara | 282 | 44 | 86 | 42 | 9.15751 | 4 | 1 | 98 | 104 | |
| 540 | Rosamunde | 301 | 81 | 127 | 62 | 9.34779 | 3 | 1 | 135 | 83 | |
| 550 | Senta | 63 | −40 | 258 | −58 | 20.5726 | 9 | 1 | 151 | 85 | |
| 553 | Kundry | 197 | 73 | 359 | 64 | 12.6025 | 5 | 1 | 61 | 80 | |
| 621 | Werdandi | 247 | −86 | 66 | −77 | 11.77456 | 12 | 2 | 146 | 71 | |
| 936 | Kunigunde | 47 | 57 | 234 | 50 | 8.82653 | | | 154 | 88 | |
| 951 | Gaspra | 20 | 23 | 198 | 15 | 7.042027 | 71 | 4 | 117 | 89 | |
| 1286 | Banachiewicza | 214 | 62 | 64 | 60 | 8.63043 | | | 81 | 51 | |
| 1353 | Maartje | 266 | 73 | 92 | 57 | 22.9926 | | | 154 | 139 | |
| 1378 | Leonce | 210 | −67 | 46 | −77 | 4.32527 | | | 89 | 113 | |
| 1423 | Jose | 78 | −82 | | | 12.3127 | | | 121 | 134 | |
| 1446 | Sillanpaa | 129 | 76 | 288 | 63 | 9.65855 | 2 | 1 | 76 | 73 | |
| 1464 | Armisticia | 194 | −54 | 35 | −69 | 7.46699 | 2 | 1 | 231 | 67 | |
| 1503 | Kuopio | 170 | −86 | 27 | −61 | 9.9586 | | | 116 | 68 | |
| 1527 | Malmquista | 274 | 80 | | | 14.0591 | | | 49 | 107 | |
| 1618 | Dawn | 39 | −60 | 215 | −51 | 43.219 | | | 93 | 91 | |
| 1633 | Chimay | 322 | 77 | 116 | 81 | 6.59064 | 2 | 1 | 127 | 83 | |
| 1691 | Oort | 45 | 68 | 223 | 58 | 10.2684 | | | 86 | 60 | |
| 1703 | Barry | 46 | −76 | 221 | −71 | 107.04 | | | 89 | 138 | |
| 1805 | Dirikis | 364 | 48 | 188 | 61 | 23.4543 | | | 117 | 91 | |
| 1835 | Gajdariya | 34 | 74 | 204 | 69 | 6.33768 | | | 66 | 86 | |
| 1987 | Kaplan | 357 | −58 | | | 9.45950 | 8 | 2 | 81 | 28 | |
| 2430 | Bruce Helin | 177 | −68 | | | 129.75 | 15 | 1 | | 112 | |
| 3279 | Solon | 268 | −70 | | | 8.1043 | 3 | 1 | | 137 | |
| 3492 | Petra-Pepi | 9 | −57 | 202 | −16 | 46.570 | 15 | 1 | 25 | 111 | |
| 4399 | Ashizuri | 266 | −48 | 45 | −61 | 2.830302 | 4 | 1 | 20 | 84 | |
| 4606 | Saheki | 44 | 59 | 222 | 68 | 4.97347 | 6 | 1 | | 123 | |
| 6159 | 1991 YH | 266 | 67 | 62 | 67 | 10.6590 | 3 | 1 | | 102 | |
| 6262 | Javid | 93 | 76 | 275 | 69 | 8.02054 | 3 | 1 | | 106 | |
| 6403 | Steverin | 246 | 77 | 109 | 73 | 3.49119 | 2 | 1 | | 74 | |
| 7043 | Godart | 73 | 62 | 235 | 80 | 8.4518 | 4 | 1 | | 121 | |
| 7169 | Linda | 11 | −60 | 198 | −61 | 27.864 | 5 | 1 | | 95 | |

**Notes.** For each asteroid, the table gives the ecliptic coordinates $\lambda_1$ and $\beta_1$ of the pole solution with the lowest $\chi^2$, the corresponding mirror solution $\lambda_2$ and $\beta_2$, the sidereal rotational period $P$, the number of dense lightcurves $N_{lc}$ observed during $N_{app}$ apparitions, and the number of sparse data points for the corresponding observatory: $N_{689}$, $N_{703}$, and $N_{950}$. The uncertainty of the sidereal rotational period corresponds to the last decimal place of $P$ and of the pole direction to 5–10° if we have multi-apparition dense data or 10–20° if the model is based mainly on sparse data (i.e., only a few dense lightcurves from 1–2 apparitions).

Asteroid Lightcurve Data Exchange Format (ALCDEF[6], Warner et al. 2009). The sparse-in-time photometry is downloaded from the AstDyS site (Asteroids – Dynamic Site[7]). We use data from the three most accurate observatories: USNO–Flagstaff station (IAU code 689), Roque de los Muchachos Observatory, La Palma (IAU code 950), and Catalina Sky Survey Observatory (CSS for short, IAU code 703, Larson et al. 2003).

To increase the number of asteroid models for our study of asteroid families, we performed additional analysis of our previous results of the lightcurve inversion. For many asteroids, we are able to determine a unique rotational period, but get multiple pole solutions (typically 3–5) with similar ecliptic latitudes $\beta$, which is an important parameter. In Hanuš et al. (2011), we presented a reliability test where we checked the physicality of derived solutions by the lightcurve inversion (i.e., if the shape model rotated around its axis with a maximum momentum of inertia). By computing models for all possible pole solutions and by checking their physicality, we removed the pole ambiguity for several asteroids, and thus determined their unique solutions (listed in Table 1). For other asteroids, the pole ambiguity remain and the models give us accurate period values and also rough estimates of ecliptic latitudes $\beta$ (if the biggest difference in latitudes of the models is <50°). We call these models *partial* and present them in Table 2. For the ecliptic latitude $\beta$, we use the mean value of all different models. We define parameter $\Delta \equiv |\beta_{max} - \beta_{min}|/2$ as being the estimated uncertainty of $\beta$, where $\beta_{max}$ and $\beta_{min}$ are the extremal values within all $\beta$. The threshold for partial models is $\Delta < 25°$.

We present 31 new models and 24 partial models. References to the dense lightcurves used for the model determination are listed in Table 3. In Sect. 4, we compare the numbers of asteroids in four quadrants of the $(a_p, \beta)$ diagram (defined by the center of the family and the value $\beta = 0°$) with the same quantities based on the synthetic family population. The uncertainties in $\beta$ are rarely greater than 20°, and the assignment to a specific quadrant is usually not questionable (only in 4 cases out of 136 does the uncertainty interval lie in both quadrants, and most of the asteroids have latitudes $|\beta| \gtrsim 30°$), and thus give us useful information about the rotational properties in asteroid families. Partial models represent about 20% of our sample of asteroid models.

[6] http://www.minorplanet.info/alcdef.html
[7] http://hamilton.dm.unipi.it/

**Table 2.** List of partial models derived from combined data sets.

| | Asteroid | $\beta$ [deg] | $\Delta$ [deg] | $P$ [hours] | $N_{lc}$ | $N_{app}$ | $N_{689}$ | $N_{703}$ |
|---|---|---|---|---|---|---|---|---|
| 391 | Ingeborg | −60 | 7 | 26.4145 | 24 | 2 | 141 | 96 |
| 502 | Sigune | −44 | 3 | 10.92667 | 9 | 2 | 157 | 52 |
| 616 | Elly | 67 | 23 | 5.29771 | 4 | 1 | 101 | 133 |
| 1003 | Lilofee | 65 | 10 | 8.24991 | | | 107 | 83 |
| 1160 | Illyria | 47 | 23 | 4.10295 | | | 96 | 100 |
| 1192 | Prisma | −65 | 14 | 6.55836 | 5 | 1 | 44 | 43 |
| 1276 | Ucclia | −49 | 22 | 4.90748 | | | 114 | 45 |
| 1307 | Cimmeria | 63 | 9 | 2.820723 | 2 | 1 | 91 | 54 |
| 1339 | Desagneauxa | 65 | 17 | 9.37510 | | | 78 | 120 |
| 1396 | Outeniqua | 62 | 7 | 3.08175 | 2 | 1 | 112 | 68 |
| 1493 | Sigrid | 78 | 7 | 43.179 | | | 78 | 103 |
| 1619 | Ueta | 39 | 6 | 2.717943 | 5 | 1 | 122 | 51 |
| 1623 | Vivian | −75 | 8 | 20.5235 | | | 77 | 58 |
| 1738 | Oosterhoff | −72 | 8 | 4.44896 | | | 109 | 105 |
| 1838 | Ursa | 47 | 17 | 16.1635 | | | 102 | 91 |
| 2086 | Newell | −60 | 12 | 78.09 | 10 | 1 | 24 | 84 |
| 3017 | Petrovic | −73 | 8 | 4.08037 | 3 | 1 | | 114 |
| 3786 | Yamada | 56 | 2 | 4.03294 | 3 | 1 | | 71 |
| 3896 | Pordenone | −32 | 9 | 4.00366 | 3 | 1 | 22 | 71 |
| 4209 | Briggs | −56 | 25 | 12.2530 | 2 | 1 | | 64 |
| 4467 | Kaidanovskij | 54 | 13 | 19.1454 | | | 20 | 107 |
| 6179 | Brett | −42 | 20 | 9.4063 | 6 | 1 | | 93 |
| 7055 | 1989 KB | −61 | 11 | 4.16878 | 7 | 1 | | 117 |
| 7360 | Moberg | −18 | 18 | 4.58533 | 3 | 1 | | 103 |

**Notes.** For each asteroid, there is the mean ecliptic latitude $\beta$ of the pole direction and its dispersion $\Delta$. The other parameters have the same meaning as in Table 1. The uncertainty of the sidereal rotational period corresponds to the last decimal place of $P$.

The typical error for the orientation of the pole is (5–10°)/cos$\beta$ in longitude $\lambda$ and 5–20° in latitude $\beta$. Both uncertainties depend on the amount, timespan, and quality of used photometry. Models based purely on dense photometry are typically derived from a large number (~30–50) of individual dense lightcurves observed during about five to ten apparitions, and thus the uncertainties of parameters of the rotational state correspond to lower values of the aforementioned range. On the other hand, models based on combined sparse-in-time data have larger uncertainties, owing to the poor photometric quality of the sparse data (corresponds to the upper bound of the aforementioned range).

Models of asteroids (281) Lucretia and (1188) Gothlandia published by Hanuš et al. (2013) were recently determined also by Kryszczyńska (2013) from partly different photometric data sets. Parameters of the rotational state for both models agree within their uncertainties.

The spin vector solution of asteroid (951) Gaspra based on Galileo images obtained during the October 1991 flyby was already published by Davies et al. (1994b). Similarly, the solution of a Koronis-family member (243) Ida based on Galileo images and photometric data was previously derived by Davies et al. (1994a) and Binzel et al. (1993). Here we present convex shape models for both these asteroids. Our derived pole orientations agree within only a few degrees with the previously published values (see Table 5), which again demonstrates the reliability of the lightcurve inversion method.

### 2.3. Family members and interlopers

We revise the family membership assignment by the HCM according to the criteria described above for interlopers or borderline cases. Interlopers are asteroids that do not clearly belong to the family; for example, they have different taxonomic types or incompatible albedos or are far from the ($a_p$, $H$) border. On the other hand, borderline cases cannot be directly excluded from the family, since their physical or orbital properties are just not typical in the context of other members (higher/lower albedos, close to the ($a_p$, $H$) border). These asteroids are possible family members, but can just as easily be interlopers. In the penultimate column of Table 5, we show our revised membership classification for each object (M is a member, I an interloper, and B a borderline case), the table also gives the rotational state of the asteroid (the ecliptic coordinates of the pole orientation $\lambda$ and $\beta$ and the period $P$), the semi-major axis $a$, the diameter $D$, and the albedo $p_V$ from WISE (Masiero et al. 2011), the SMASS II (Bus & Binzel 2002), and Tholen (Tholen 1984, 1989) taxonomic types, and the reference to the model).

Although we got several members by the HCM for Vesta and Nysa/Polana families, we excluded these two families from further study of spin states. The Vesta family was created by a cratering event, and thus a majority of the fragments are rather small and beyond the capabilities of the model determination. Most of the models we currently have (recognized by the HCM) are not compatible with the SFD of the Vesta family and thus are interlopers. On the other hand, Nysa/Polana family is a complex of two families (of different age and composition), hence should be treated individually. Additionally, we only have five member candidates for the whole complex, so even if we assign them to the subfamilies, the numbers would be too low to make any valid conclusions.

In Table 4, we list asteroids for which the HCM suggested a membership in families Flora, Koronis, Eos, Eunomia, Phocaea and Alauda, but using the additional methods for the family membership determination described above, we identified them as interlopers or borderline cases. In Fig. 3, we show the ($a_p$, $H$)

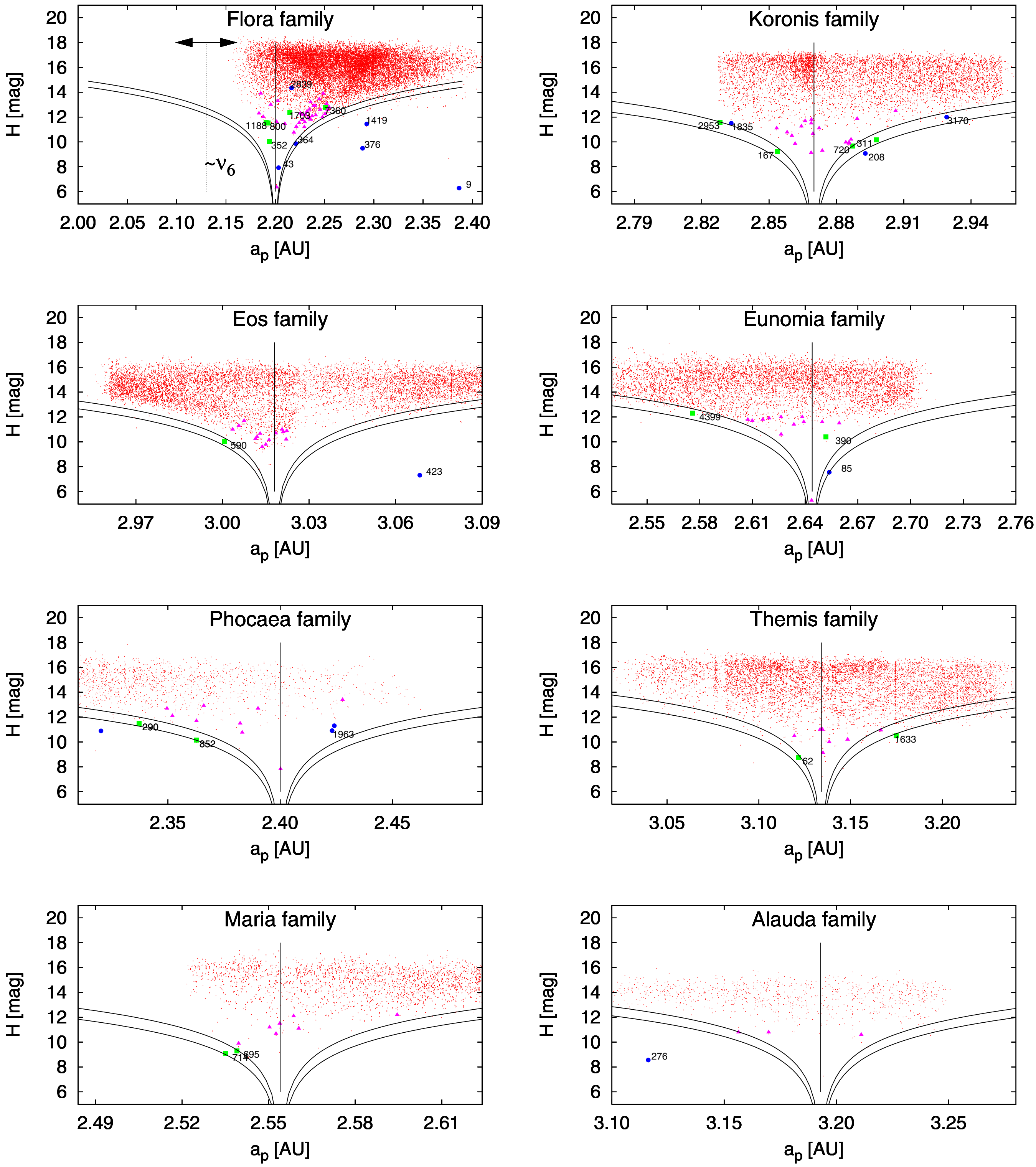


**Fig. 3.** Dependence of the absolute magnitude $H$ on the proper semi-major axis $a_p$ for the eight families: Flora, Koronis, Eos, Eunomia, Phocaea, Themis, Maria and Alauda with the likely positions of the family centers (vertical lines). We also plot the possible range of the ($a_p$, $H$) borders (two thick lines) of each family for values of the parameter $C$ from Brož et al. (2013) (different values correspond to a different initial extent of the family or different age and magnitude of the Yarkovsky semi-major axis drift.). The pink triangles represent the members from our sample (M), green circles borderline cases (B) and blue circles interlopers (I). Borderline cases and interlopers are identified by several methods including the position in the ($a_p$, $H$) diagram, and thus could also lie close to the center of the family (e.g., in the case of the Flora family).

diagrams for all eight studied families. We plotted the adopted ($a_p$, $H$) border (from Brož et al. 2013) and labeled the members, borderline cases, and interlopers by different colors.

Several asteroids in our sample belong to smaller and younger subclusters within the studied families (e.g., (832) Karin in the Koronis family, (1270) Datura in the Flora family, or (2384) Schulhof in the Eunomia family). These subclusters were probably created by secondary collisions. As a result, the spin states of asteroids in these subclusters were randomly reoriented. Because our combined orbital- and spin-evolution model (see Sect. 4) includes secondary collisions (reorientations), using asteroids from subclusters in the study of the spin-vector distribution is thus essential: asteroids from subclusters correspond to reoriented asteroids in our synthetic population.

## 3. Observed spin vectors in families

There are eight asteroid families for which we find at least three members (together with borderline cases) in our data set of asteroid models (after the family membership revision, labeled by M or B in the last column of Table 5) – Flora (38 members), Koronis (23), Eos (16), Eunomia (14), Phocaea (11), Themis (9), Maria (9), and Alauda (3) families. Now that we have the models and membership, we can proceed to the discussion of the spin states in families in general (Sect. 3.1), and for families Flora and Koronis (Sects. 3.2, 3.3).

### 3.1. Spin-vector orientations in individual families

In Fig. 4, we show the dependence of asteroid's pole latitudes in ecliptic coordinates on the semi-major axes. If there are two possible pole solutions for an asteroid, we take the first one in Table 1, because it corresponds to a formally better solution, additionally, latitudes for both ambiguous models are usually similar. To determine the centers of families, we use all members of each family assigned by the HCM, see Figs. 1 and 3. The Eos family has an asymmetric V-shape (the ($a_p$, $H$) diagram), so we compute centers for both wings of the V-shape individually. For the Flora family, we use only the right wing of the V-shape to derive the center, while the left one is strongly affected by the $\nu_6$ secular resonance.

In the study of spin-vector properties in families, we simply use the ecliptic coordinates for the pole orientation: ecliptic longitude $\lambda$ and latitude $\beta$. A formally better approach would be to use the coordinates bound to the orbital plane of the asteroid: orbital longitude $\lambda_{\mathrm{orb}}$ and latitude $\beta_{\mathrm{orb}}$. The orbital latitude can then be easily transformed to obliquity, which directly tells us whether the asteroid rotates in a prograde or retrograde sense. However, for several reasons, we prefer the ecliptic coordinates: (i) most of the asteroids have low inclinations and thus the differences between their ecliptic and orbital latitudes are only a few degrees, and the maximum differences for the families with higher inclination (Eos, Eunomia, Phocaea, Maria) are 20–30°; (ii) the orbital coordinates of the pole direction cannot be computed for partial models, because we do not know the ecliptic longitude, these models represent about 20% of our studied sample; (iii) the positions of the asteroids in the ($a_p$, $\beta$) diagrams (i.e., to which quadrant they belong), namely if they have $\beta > 0°$ or $\beta < 0°$, are sufficient information. Because most of the asteroids have latitudes larger than 30°, their positions in the ($a_p$, $\beta_{\mathrm{orb}}$) are similar (not true only for three asteroids out of 136); and (iv) we compare the ($a_p$, $\beta$) diagrams (numbers of objects in the quadrants) between the observed and synthetic populations for ecliptic latitudes, so the consistency is assured.

In general, we observe similar trends for all studied families: (i) larger asteroids are situated in the proximity of the center of the family; (ii) asteroids with $\beta > 0°$ are usually found to the right of the family center; (iii) asteroids with $\beta < 0°$ are to the left of the center; (iv) the majority of asteroids have large pole-ecliptic latitudes ($|\beta| \gtrsim 30°$); and finally (v) some families have a statistically significant excess of asteroids with $\beta > 0°$ or $\beta < 0°$.

Case (i) is evident for families Flora, Eunomia, Phocaea, Themis, or Maria. We have no large asteroids in the samples for the remaining families.

Cases (ii) and (iii) are present among all families with the exception of Eos, where all the asteroids are close to the (badly constrained) center. This phenomenon can be easily explained by the Yarkovsky drift, which can change asteroid's semi-major axes $a$; that is, it can increase $a$ of prograde rotators, and decrease $a$ of retrograde once. The magnitude of the Yarkovsky drift is dependent on the asteroid size, is negligible for asteroids with diameters $D \gtrsim 50$ km (the case of Eos), and increases with decreasing diameter. For the Flora, Eunomia, Phocaea, or Maria families, we can see that the smallest asteroids in the sample ($D \sim 5$–10 km) can be situated far from the family center, and we can also notice a trend toward decreasing size with increasing distance from the center that probably corresponds to the magnitude of the Yarkovsky effect and the initial velocities $v_{\mathrm{ini}}(D)$ that the objects gained after the break-up.

Observation (iv) is a result of the dynamical evolution of the asteroid's spin vector orientations dominated by the YORP effect, which increases the absolute value of the pole-ecliptic latitude. See papers Hanuš et al. (2011, 2013), where this effect is numerically investigated and compared with the observed anisotropic spin vector distribution of the sample of ~300 MBAs.

Case (v) concerns families Flora, Eunomia, Phocaea, Themis, and Maria. The different number of asteroids with $\beta > 0°$ and $\beta < 0°$ among these families is statistically significant and cannot be coincidental. The obvious choice for an explanation are mean-motion or secular resonances. Indeed, the $\nu_6$ secular resonance removed many objects with $\beta > 0°$ from the Flora family (see Sect. 3.2 for a more thorough discussion). The 8:3 resonance with Jupiter truncated the Eunomia family, which resulted in there being no objects with $a_p > 2.70$ AU; similarly, the 3:1 resonance with Jupiter affected the Maria family, for which we do not observe objects with smaller $a_p$ than 2.52 AU. The 3:1 resonance with Jupiter is situated near the Phocaea family at $a = 2.50$ AU. Due to the high inclination of objects in the Phocaea family ($I \sim 24°$), the resonance affects asteroids with $a_p > 2.40$ AU, which corresponds to the probable center of the family. The resonance removed a significant number of objects between 2.40 AU and 2.45 AU, and all objects with larger $a_p$.

The asymmetry of asteroids with $\beta > 0°$ and $\beta < 0°$ in the Themis family is caused by a selection effect: in the family, there are no objects with absolute magnitude $H < 12$ mag (i.e., large asteroids) and $a_p < 3.10$ AU. On the other hand, with $a_p > 3.10$ AU, there are more than a hundred such asteroids (see Fig. 1a). Our sample of asteroid models derived by the lightcurve inversion method is dominated by larger asteroids, so it is not surprising that we did not derive models for the Themis family asteroids with $a_p < 3.10$ AU. The Flora and Koronis families are also interesting for other aspects, and thus are discussed in more detail in Sects. 3.2 and 3.3.

### 3.2. The Flora family

The Flora cluster is situated in the inner part of the main belt between 2.17–2.40 AU, and its left part (with respect to the ($a_p$, $H$) diagram) is strongly affected by the secular $\nu_6$ resonance with Saturn, which is demonstrated in Fig. 1b. The probable center of the family matches the position of asteroid (8) Flora at $a = 2.202$ AU. Because of the relative proximity to the Earth,

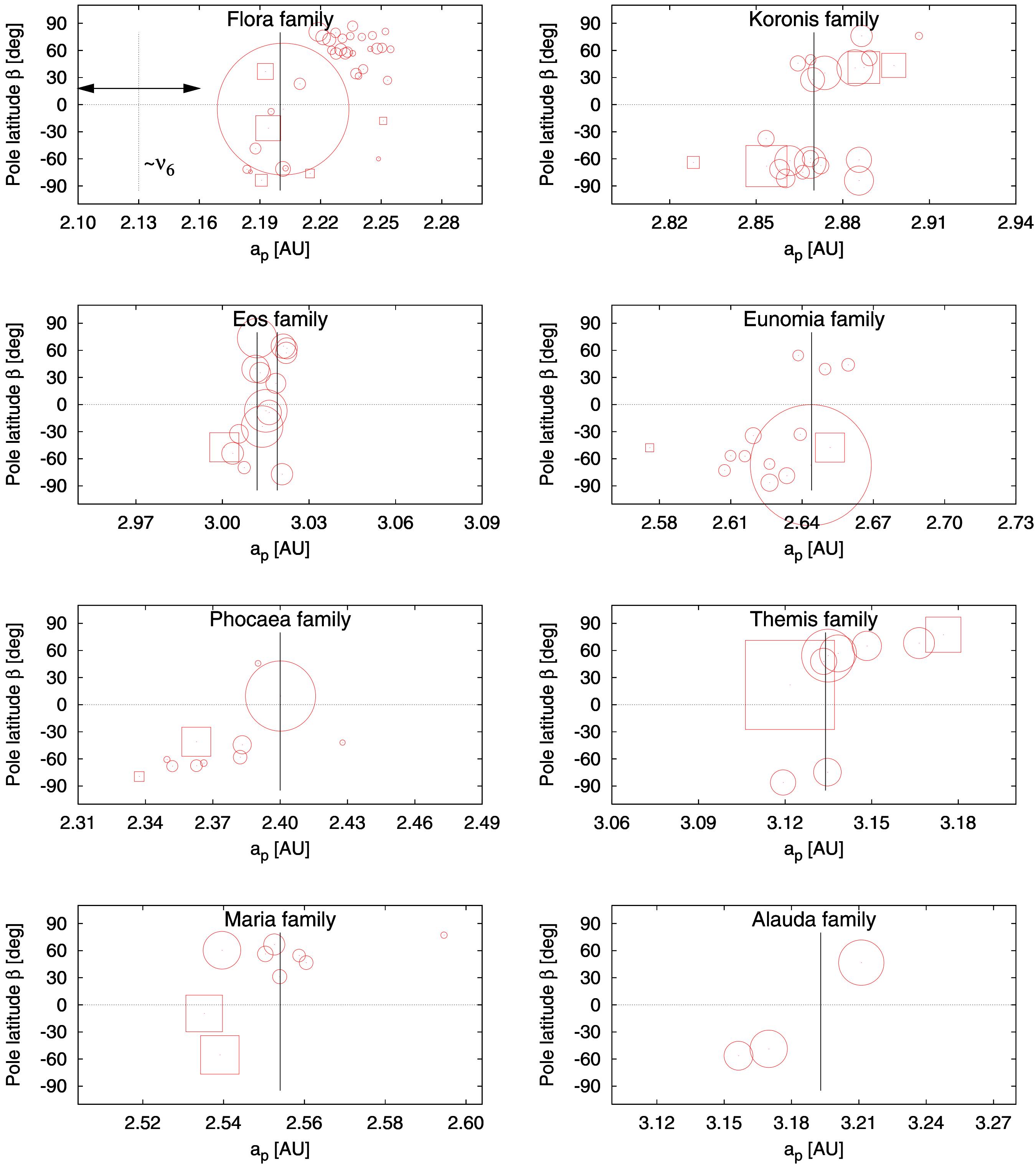


**Fig. 4.** Dependence of the pole latitude $\beta$ on the proper semi-major axis $a_p$ for eight studied asteroid families: Flora, Koronis, Eos, Eunomia, Phocaea, Themis, Maria, and Alauda. Family members are marked by circles and borderline cases by squares, whose sizes are scaled proportionally to diameters. Only the scale for (15) Eunomia was decreased by half to fit the figure. The vertical lines correspond to the likely centers of the asteroid families, whose uncertainties are usually <0.01 AU. The Eos family has an asymmetric V-shape (the ($a_p$, $H$) border is asymmetric), which makes the center determination harder, so we marked two possible positions. One corresponds to the right ($a_p$, $H$) border, the second to the left border. The uncertainties in $\beta$ are usually 5–20°. In most cases, the value of $|\beta| \gtrsim 30°$, hence the quadrant to which the asteroid belongs (defined by the center of the family and the value $\beta = 0°$), is *not* changed.

more photometric measurements of smaller asteroids are available than for more distant families, and thus more models were derived. So far, we identified 38 models of asteroids that belong to the Flora family (together with borderline cases).

The majority of asteroids within this family have $\beta > 0°$ (∼68%; due to small inclinations of the family members, the majority of the objects with $\beta > 0°$ are definitely prograde rotators, because their obliquities are between 0° and 90°) and lie to the right of the center of the family, confirming the presence of the Yarkovsky drift. Nine out of twelve asteroids with $\beta < 0°$ can be found in Fig. 4 near to or to the left of the center of the family. The exceptions are the borderline asteroids (1703) Barry and (7360) Moberg, and asteroid (7169) Linda with $a_\mathrm{p}$ close to 2.25 AU (see Fig. 4). The borderline category already suggests that the two asteroids could be possible interlopers, and their rotational state seems to support this statement. However, it is also possible that these asteroids have been reoriented by noncatastrophic collisions. The rotational state of another borderline asteroid (800) Kressmannia also does not agree with the Yarkovsky/YORP predictions, so it could be an interloper (or reoriented). The asteroid (7169) Linda classified as a member could still be an interloper, which was not detected by our methods for interloper removal, or could have recently been reoriented by a noncatastrophic collision. The typical timescale for a reorientation (Farinella et al. 1998, see Eq. (5)) of this 4km-sized asteroid with rotational period $P = 27.9$ h is $\tau_\mathrm{reor} \sim 500$ Myr, which is comparable to the age of the family. The depopulation of poles close to the ecliptic plane is also clearly visible.

The $\nu_6$ resonance to the left of the center of the family creates an excess of retrograde rotators not only among the family, but also among the whole main belt population if we use the currently available sample of asteroid models (there are ∼300 asteroid models in the DAMIT database). In the Flora family, there are 14 more asteroids with $\beta > 0°$ than with $\beta < 0°$ (i.e, we have a prograde excess), which corresponds to about 6% of the whole sample. This bias needs to be taken into consideration, for example, in the study of rotational properties among MBAs.

The missing asteroids with $\beta < 0°$ were delivered by this resonance to the orbits crossing the orbits of terrestrial planets and are responsible, for example, for the retrograde excess of the NEAs (La Spina et al. 2004). The $\nu_6$ resonance contributes to the NEA population only by retrograde rotators, and other major mean-motion resonances, such as the 3:1 resonance with Jupiter, deliver both prograde and retrograde rotators in a similar amount.

We did not observe a prograde group of asteroids with similar pole-ecliptic longitudes in the Flora family (i.e., a direct analog of the Slivan state in the Koronis family) that was proposed by Kryszczyńska (2013). Although Kryszczyńska (2013) claims that Slivan states are likely to be observed in the Flora family, no corresponding clustering of poles of the prograde rotators is shown, particularly for ecliptic longitudes. We believe that the term *Slivan state* was used incorrectly there.

### 3.3. The Koronis family

The Koronis family is located in the middle main belt between 2.83–2.95 AU with the center at $a = 2.874$ AU. We identified 23 members (together with borderline cases) with determined shape models. The concept given by the Yarkovsky and YORP predictions also work among the Koronis family (asteroids with $\beta < 0°$ lie to the left from the family center, asteroids with $\beta > 0°$ to the right, see Fig. 4). In addition to that, Slivan (2002) and Slivan et al. (2003) noticed that prograde rotators have also clustered pole longitudes. These asteroids were trapped in a secular spin-orbital resonance $s_6$ and are referred to as being in Slivan states (Vokrouhlický et al. 2003). Several asteroids were later recognized as being incompatible with the Slivan states, such as (832) Karin and (263) Dresda by Slivan & Molnar (2012). Asteroid (832) Karin is the largest member of a young (∼5.8 Myr, Nesvorný & Bottke 2004) collisional family that is confined within the larger Koronis family. The spin state of (832) Karin was thus probably affected during this catastrophic event and changed to a random state. Asteroid (263) Dresda could be randomly reoriented by a noncatastrophic collision that is likely to happen for at least a few of 27 asteroids in the Koronis cluster with known spin state solutions, or its initial rotational state and shape did not allow a capture in the resonance. All four borderline asteroids have rotational states that agree with the Yarkovsky/YORP concept, which may support their membership in the Koronis cluster. On the other hand, rotational states of asteroids (277) Elvira and (321) Florentina do not match the expected values, and thus could again be interlopers or be affected by reorientations.

Being trapped in the spin-orbital resonance does not necessarily mean that the asteroid is a member of the Koronis family. It rather indicates that its initial orbital position, the rotational state, and the shape were favorable to being trapped in the resonance. For example, asteroids (311) Claudia, (720) Bohlinia, (1835) Gajdariya, and (3170) Dzhanibekov have expected rotational states but are either rejected from the Koronis family or classified as borderline cases by our membership revision.

## 4. Long-term evolution of spin vectors in asteroid families

Here we present a comparison of the observed spin-vector orientations in several asteroid families with a numerical model of the temporal spin-vector evolutions. We used a *combined* orbital- and spin-evolution model, which was described in detail in Brož et al. (2011). We need to account for the fact that the Yarkovsky semi-major axis drift is sensitive to the orientation of the spin axis, which is in turn affected by the YORP effect and nondisruptive collisions. This model includes the following processes, which are briefly described in the text: (i) impact disruption; (ii) gravitational perturbations of planets; (iii) the Yarkovsky effect; (iv) the YORP effect; (v) collisions and spin-axis reorientations; and (vi) mass shedding.

Impact disruption. To obtain initial conditions for the family just after the breakup event, we used a very simple model of an isotropic ejection of fragments from the work of Farinella et al. (1994). The distribution of velocities "at infinity" follows the function

$$\mathrm{d}N(v)\mathrm{d}v = C' v \left(v^2 + v_\mathrm{esc}^2\right)^{-(\alpha+1)/2} \mathrm{d}v, \qquad (1)$$

with the exponent $\alpha$ as a free parameter, $C'$ a normalization constant and $v_\mathrm{esc}$ the escape velocity from the parent body, which is determined by its size $D_\mathrm{PB}$ and mean density $\rho_\mathrm{PB}$ as $v_\mathrm{esc} = \sqrt{(2/3)\pi G \rho_\mathrm{PB}}\, D_\mathrm{PB}$. The distribution is usually cut at a selected maximum-allowed velocity $v_\mathrm{max}$ to prevent outliers. The initial velocities $|v|$ of individual bodies are generated by a straightforward Monte-Carlo code, and the orientations of the velocity vectors $\boldsymbol{v}$ in space are assigned randomly. We also assume that the velocity of fragments is independent of their size.

We must also select initial osculating eccentricity $e_\mathrm{i}$ of the parent body, initial inclination $i_\mathrm{i}$, as well as true anomaly $f_\mathrm{imp}$ and argument of perihelion $\omega_\mathrm{imp}$ at the time of impact disruption, which determine the initial shape of the synthetic family just after the disruption of the parent body.

**Gravitational perturbations of planets.** Orbital integrations were performed using the SWIFT package (Levison & Duncan 1994), slightly modified to include necessary online digital filters and a second-order symplectic integrator (Laskar & Robutel 2001). The second-order symplectic scheme allows us to use a timestep up to $\Delta t = 91$ d.

Our simulations included perturbations by four outer planets, with their masses, initial positions and velocities taken from the JPL DE405 ephemeris (Standish et al. 1997). We modified the initial conditions of the planets and asteroids by a barycentric correction to partially account for the influence of the terrestrial planets. The absence of the terrestrial planets as perturbers is a reasonable approximation in the middle and outer parts of the main belt (for orbits with $a > 2.5$ AU and $e < 0.6$)[8].

Synthetic proper elements are computed as follows. We first apply a Fourier filter to the (nonsingular) orbital elements in a moving window of 0.7 Myr (with steps of 0.1 Myr) to eliminate all periods smaller than some threshold (1.5 kyr in our case). We use a sequence of Kaiser windows as in Quinn et al. (1991).

The filtered signal, which are mean orbital elements, is then passed through a frequency analysis code adapted from Šidlichovský & Nesvorný (1996) to obtain (planetary) forced and free terms in Fourier representation of the orbital elements. The isolated free terms are what we use as the proper orbital elements.

**Yarkovsky effect.** Both diurnal and seasonal components of the Yarkovsky accelerations are computed directly in the $N$-body integrator. We used a theory of Vokrouhlický (1998) and Vokrouhlický & Farinella (1999) for spherical objects (but the magnitude of the acceleration does not differ substantially for nonspherical shapes Vokrouhlický & Farinella 1998). The implementation within the SWIFT integrator is described in detail by Brož (2006).

**YORP effect.** The evolution of the orientation of the spin axis and of the angular velocity is given by

$$\frac{\mathrm{d}\omega}{\mathrm{d}t} = c f_i(\epsilon), \qquad i = 1\ldots200, \tag{2}$$

$$\frac{\mathrm{d}\epsilon}{\mathrm{d}t} = c\frac{g_i(\epsilon)}{\omega}, \tag{3}$$

where $f$- and $g$-functions describing the YORP effect for a set of 200 shapes were calculated numerically by Čapek & Vokrouhlický (2004) with the effective radius $R_0 = 1$ km and the bulk density $\rho_0 = 2500\,\mathrm{kg/m^3}$, located on a circular orbit with the semi-major axis $a_0 = 2.5$ AU. We assigned one of the artificial shapes (denoted by the index $i$) to each individual asteroid from our sample. The $f$- and $g$-functions were then scaled by the factor

$$c = c_{\mathrm{YORP}}\left(\frac{a}{a_0}\right)^{-2}\left(\frac{R}{R_0}\right)^{-2}\left(\frac{\rho_{\mathrm{bulk}}}{\rho_0}\right)^{-1}, \tag{4}$$

where $a$, $R$, and $\rho_{\mathrm{bulk}}$ denote the semi-major axis, the radius, and the density of the simulated body, respectively, and $c_{\mathrm{YORP}}$ is a free scaling parameter reflecting our uncertainty in the shape models and the magnitude of the YORP torque, which depends on small-sized surface features (even boulders, Statler 2009) and other simplifications in the modeling of the YORP torque. In Hanuš et al. (2013), we constrained this parameter and find $c_{\mathrm{YORP}} = 0.2$ to be the optimal value when comparing the results of the simulation with the observed latitude distribution of main belt asteroids. In our simulation, we used this value for $c_{\mathrm{YORP}}$.

The differential Eqs. (2) and (3) are integrated numerically by a simple Euler integrator. The usual time step is $\Delta t = 1000$ yr.

**Collisions and spin-axis reorientations.** We neglected the effect of disruptive collisions because we do not want to lose objects during the simulation, but we included spin axis reorientations caused by collisions. We use an estimate of the timescale by Farinella et al. (1998).

$$\tau_{\mathrm{reor}} = B\left(\frac{\omega}{\omega_0}\right)^{\beta_1}\left(\frac{D}{D_0}\right)^{\beta_2}, \tag{5}$$

where $B = 84.5$ kyr, $\beta_1 = 5/6$, $\beta_2 = 4/3$, $D_0 = 2$ m, and $\omega_0$ corresponds to period $P = 5$ h. These values are characteristic of the main belt.

**Mass shedding.** If the angular velocity approaches a critical value

$$\omega_{\mathrm{crit}} = \sqrt{\frac{4}{3}\pi G\rho_{\mathrm{bulk}}}, \tag{6}$$

we assume a mass shedding event, so we keep the orientation of the spin axis and the sense of rotation, but we reset the orbital period $P = 2\pi/\omega$ to a random value from the interval $(2.5, 9)$ h. We also change the assigned shape to a different one, since any change in shape may result in a different YORP effect.

**Synthetic Flora, Koronis, and Eos families.** In Fig. 5 (top panel), we show a long-term evolution of the synthetic Flora family in the proper semi-major axis $a_{\mathrm{p}}$ vs. the pole latitude $\beta$ plane for objects larger and smaller than 30 km. The values of the model parameters are listed in the figure caption. Larger asteroids do not evolve significantly and remain close to their initial positions. On the other hand, smaller asteroids ($D < 30$ km) are strongly affected by the Yarkovsky and YORP effects: They drift in the semi-major axis, differently for prograde and retrograde rotators, and their pole orientations become mostly perpendicular to their orbits (corresponding to the proximity of the ecliptic plane for small inclinations). After the simulation at $t = 1$ Gyr, we observe a deficiency of asteroids with $\beta > 0°$ to the left of the family center and a deficiency of asteroids with $\beta < 0°$ to the right of the family center.

The asymmetry of the synthetic Flora family with respect to its center (Fig. 5) caused by the secular $\nu_6$ resonance is obvious. The own-right hand quadrant ($\beta < 0°$, $a_{\mathrm{p}} > 2.202$ AU) still contains many objects for $t = 1$ Gyr, because for some of them the evolution in $\beta$ and $a_{\mathrm{p}}$ is rather small, and others were delivered to this quadrant by collisional reorientations.

The appearance of the evolved proper semi-major axis $a_{\mathrm{p}}$ vs. the pole latitude $\beta$ diagrams for Koronis and Eos families are qualitatively similar to the one of the Flora family. Because the asteroid samples for Koronis and Eos families are dominated by intermediate-sized asteroids ($D \sim 20$–$50$ km), the evolution in $a_{\mathrm{p}}$ and $\beta$ is on average slower than in the Flora family. We show the state of the simulation for Koronis family in 4 Gyr and

[8] For the Flora family located in the inner belt, we should account for terrestrial planets directly, because of mean-motion resonances with Mars, but we decided not do so to speed the computation up. Anyway, the major perturbation we need to account for is the $\nu_6$ secular resonance, which is indeed present in our model.

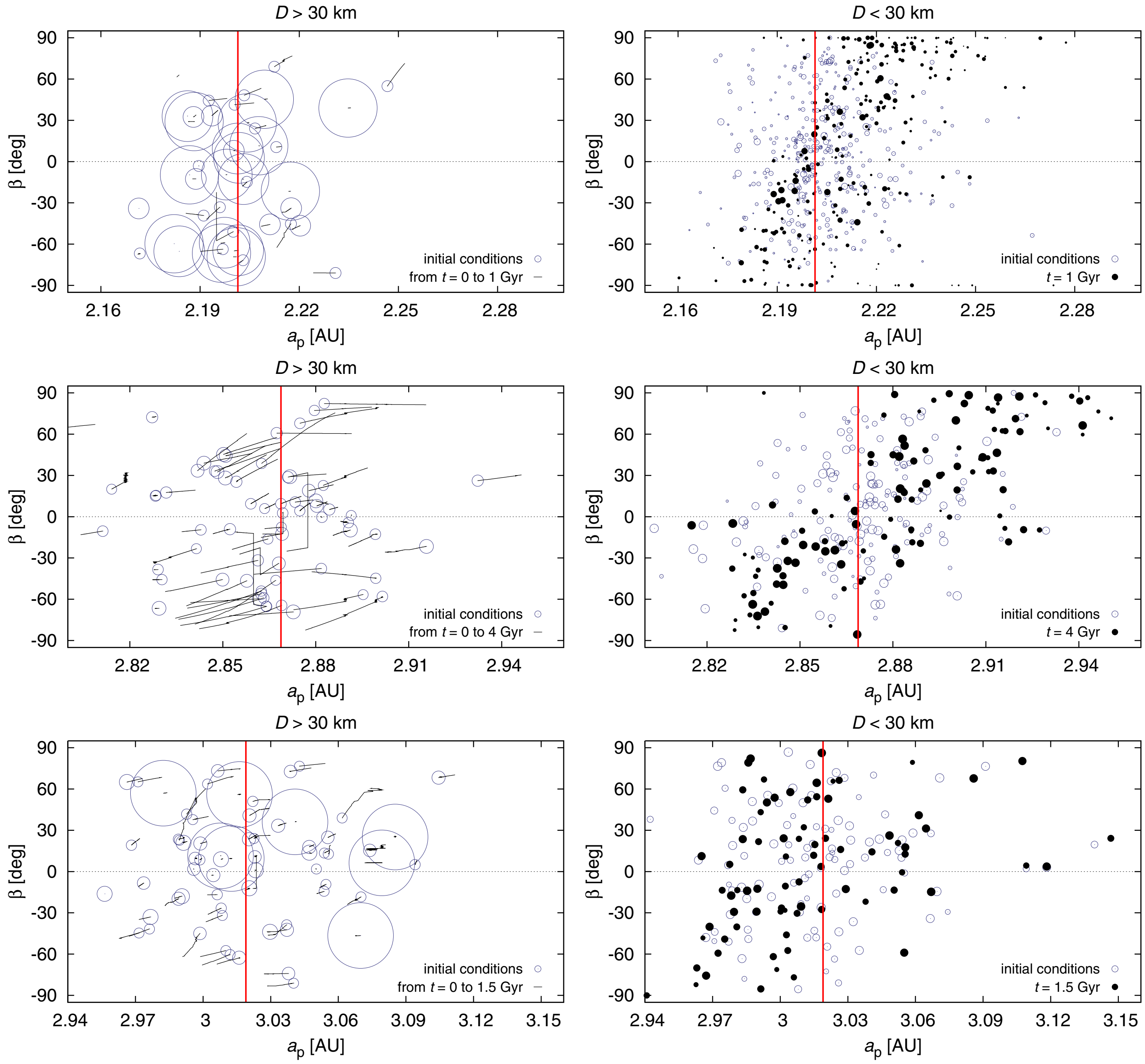


**Fig. 5.** A simulation of the long-term evolution of the synthetic Flora (*top*), Koronis (*middle*) and Eos (*bottom*) families in the proper semi-major axis $a_\mathrm{p}$ vs. the pole latitude $\beta$ plane. *Left*: objects larger than $D > 30$ km, which almost do not evolve in $\beta$. *Right*: objects with $D \leq 30$ km, with the initial conditions denoted by empty circles and an evolved state at 1 Gyr denoted by full circles. The sizes of symbols correspond to the actual diameters $D$. The initial conditions for Flora correspond to an isotropic size-independent velocity field with $\alpha = 3.25$ and $v_\mathrm{esc} = 95\,\mathrm{m\,s^{-1}}$, and a uniform distribution of poles (i.e. $\sin\beta$). We increase the number of objects 10 times compared to the observed members of the Flora (Koronis and Eos as well) family to improve statistics. We retain their size distribution, of course. The objects in Flora family are discarded from these plots when they left the family region (eccentricity $e_\mathrm{p} = 0.1$ to 0.18, inclination $\sin I_\mathrm{p} = 0.05$ to 0.13), because they are affected by strong mean-motion or secular resonances ($\nu_6$ in this case). Thermal parameters were set as follows: the bulk density $\rho_\mathrm{bulk} = 2500\,\mathrm{kg\,m^{-3}}$, the surface density $\rho_\mathrm{surf} = 1500\,\mathrm{kg\,m^{-3}}$, the thermal conductivity $K = 0.001\,\mathrm{W\,m^{-1}\,K^{-1}}$, the thermal capacity $C_\mathrm{t} = 680\,\mathrm{J\,kg^{-1}}$, the Bond albedo $A = 0.1$, and the infrared emissivity $\epsilon = 0.9$. The time step for the orbital integration is $\mathrm{d}t = 91$ days and $\mathrm{d}t_\mathrm{spin} = 10^3$ yr for the (parallel) spin integration. The parameters for Koronis and Eos are chosen similarly, only for Koronis do we use $v_\mathrm{esc} = 100\,\mathrm{m\,s^{-1}}$, and $v_\mathrm{esc} = 225\,\mathrm{m\,s^{-1}}$ and $\rho_\mathrm{surf} = 2500\,\mathrm{kg\,m^{-3}}$ for Eos.

for Eos in 1.5 Gyr (based on the expected ages). The Eos family thus seems less evolved than the Koronis family.

We also checked the distributions of the proper eccentricities and inclinations of the synthetic Flora/Koronis/Eos objects for whether they (at least roughly) correspond to the observed family. However, the number of objects to compare is fairly low and seems insufficient for any detailed comparison of distributions in 3D space of proper elements ($a_\mathrm{p}$, $e_\mathrm{p}$, $\sin I_\mathrm{p}$).

Ages of the Flora, Koronis, and Eos families. To quantitatively compare the simulation of the long-term evolution of the synthetic families in the proper semi-major axis $a_\mathrm{p}$ vs. the pole latitude $\beta$ plane with the observation, we constructed the following metric: we divide the $(a_\mathrm{p}, \beta)$ plane into four quadrants defined by the center of the family and value $\beta = 0°$ and compute the ratio $(k_2 + k_4)/(k_1 + k_3)$, where $k_i$ correspond to the numbers of synthetic objects in quadrants $i$ ($i = 1, 2, 3, 4$). In Fig. 6, we show the

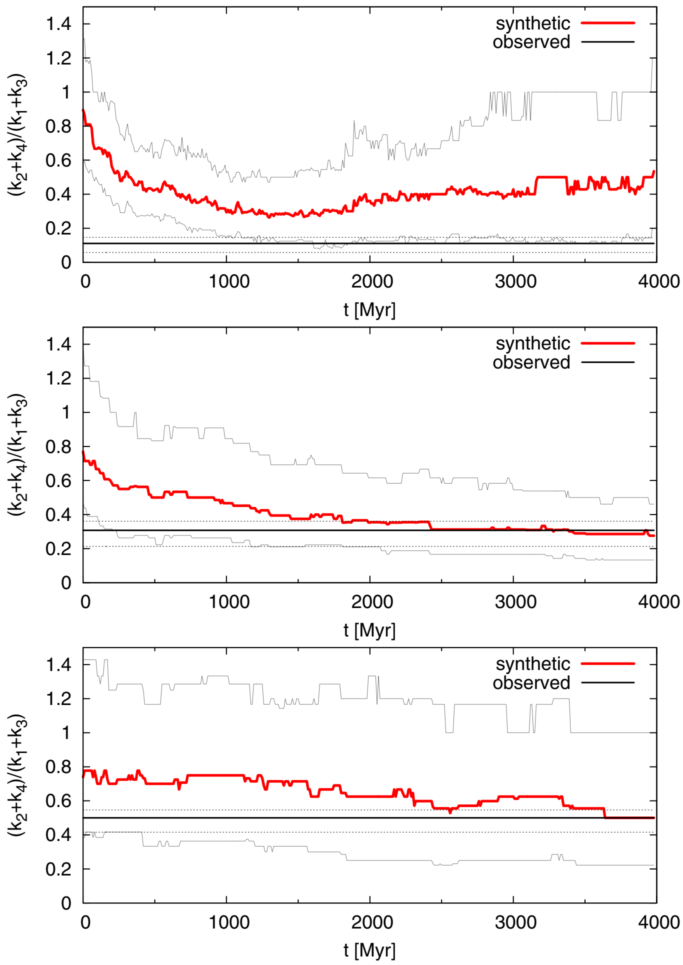


**Fig. 6.** Time evolution of the metric $(k_2 + k_4)/(k_1 + k_3)$, where $k_i$ correspond to the numbers of synthetic objects in quadrants $i$ $(i = 1, 2, 3, 4)$ that are defined by the center of the family and value $\beta = 0°$, for synthetic Flora, Koronis, and Eos families (red lines). The spread corresponds to 100 different selections of objects (we simulate 10 times more objects to reach a better statistics). the upper curve denotes the 90% quantile and the bottom 10%. Thick horizontal line is the observed ratio $(k_2 + k_4)/(k_1 + k_3)$ with the uncertainty interval.

evolution of the metric $(k_2 + k_4)/(k_1 + k_3)$ during the simulation of families Flora, Koronis, and Eos for all synthetic objects with $D < 30$ km, and the value of the same metric for the observed population for comparison.

For the Koronis family (middle panel), the synthetic ratio reaches the observed one after $t = 2.5$ Gyr and remains similar until the end of the simulation at $t = 4$ Gyr. Bottke et al. (2001) published the age $t = (2.5 \pm 1.0)$ Gyr for the Koronis family. Unfortunately, we cannot constrain the age of the Eos family from this simulation owing to objects with the relatively small evolution in $a_p$ and $\beta$. The fit for the Flora family is not ideal, and the reason could be differences in the initial velocity field or the true anomaly $f_{imp}$ of the impact. The best agreement is for the age $t = (1.0 \pm 0.5)$ Gyr, which is approximately in agreement with the dynamical age in Nesvorný et al. (2005): $(1.5 \pm 0.5)$ Gyr.

## 5. Conclusions

We have identified 152 asteroids for which we have convex shape models, and simultaneously the HCM identifies them as members of ten collisional families. Owing to a large number of expected interlopers in families Vesta and Nysa/Polana, we excluded these families from the study of the rotational properties. In the remaining sample of asteroids from eight families, we identified ∼20% of objects that are interlopers or borderline cases (see Table 4). We used several methods, described in Sect. 2.1, for their identification. The borderline cases are still possible members of the families and thus were included in our study of the spin-vector distribution.

From the dependence of the asteroid's pole latitudes on the semi-major axes, plotted in Fig. 4, we can see fingerprints of families spreading in $a$ and spin axis evolution due to Yarkovsky and YORP effects: Asteroids with $\beta < 0°$ lie on the left side of the center of the family, and asteroids with $\beta > 0°$ on the right side. The asymmetry with respect to the family centers is in most cases caused by various resonances that cut the families, and in the case of Themis family, a selection effect is responsible.

However, we did not observe *perfect* agreement with the Yarkovsky and YORP effects predictions. A few individual objects (eight) that have incompatible rotational states could (i) be incorrectly determined; (ii) be interlopers; (iii) have initial rotational states that only cause a small evolution in the $(a_p, \beta)$ space (i.e., they are close to their initial positions after the break-up); or (iv) be recently reoriented by collisional events.

In the case of the Flora family, significantly fewer asteroids with $\beta < 0°$ (∼32%) than with $\beta > 0°$ (∼68%) are present. The secular $\nu_6$ resonance is responsible for this strong deficit, because objects with $\beta < 0°$ are drifting towards this resonance and are subsequently removed from the family. They become part of the NEAs population where they create an excess of retrograde rotators. We did not find any analog of the Slivan states (observed in the Koronis family) among any other of the studied families.

We simulated a long-term evolution of the synthetic Flora, Koronis, and Eos families (Fig. 5) in the proper semi-major axis $a_p$ vs the pole latitude $\beta$ plane and compared the results with the properties of observed asteroid families. We obtained a good qualitative agreement between the observed and synthetic spin-vector distributions. For all three families, we computed evolution of the number of objects in the four quadrants of the families in the $(a_p, \beta)$ diagram, and we estimated ages for families Flora $(1.0 \pm 0.5)$ Gyr and Koronis (2.5 to 4 Gyr) that agree with previously published values. However, we did not estimate the age of the Eos family due to a small evolution of the objects in the $(a_p, \beta)$ diagram.

The uncertainties seem to be dominated by the observed quadrant ratios. We expect that increasing the sample size by a factor of 10 would decrease the relative uncertainty by a factor of about 3, which is a good motivation for further work on this subject.

*Acknowledgements.* The work of J.H. and J.D. has been supported by grants GACR P209/10/0537 and P209/12/0229 of the Czech Science Foundation, and the work of J.D. and M.B. by the Research Program MSM0021620860 of the Czech Ministry of Education. The work of M.B. has been also supported by grant GACR 13-013085 of the Czech Science Foundation.

## References

Binzel, R. P., Slivan, S. M., Magnusson, P., et al. 1993, Icarus, 105, 310
Bottke, W. F., Vokrouhlický, D., Brož, M., Nesvorný, D., & Morbidelli, A. 2001, Science, 294, 1693
Bottke, J. W. F., Vokrouhlický, D., Rubincam, D. P., & Nesvorný, D. 2006, Ann. Rev. Earth Planet. Sci., 34, 157
Brinsfield, J. W. 2008a, Minor Planet Bulletin, 35, 179
Brinsfield, J. W. 2008b, Minor Planet Bulletin, 35, 119
Brinsfield, J. W. 2009, Minor Planet Bulletin, 36, 127

Brož, M. 2006, Ph.D. Thesis, Charles University in Prague
Brož, M., Vokrouhlický, D., Morbidelli, A., Nesvorný, D., & Bottke, W. F. 2011, MNRAS, 414, 2716
Brož, M., Morbidelli, A., Bottke, W. F., et al. 2013, A&A, 551, A117
Bus, S. J., & Binzel, R. P. 2002, Icarus, 158, 146
Čapek, D., & Vokrouhlický, D. 2004, Icarus, 172, 526
Davies, M. E., Colvin, T. R., Belton, M. J. S., et al. 1994a, in AAS/Division for Planetary Sciences Meeting Abstracts #26, BAAS, 26, 1154
Davies, M. E., Colvin, T. R., Belton, M. J. S., Veverka, J., & Thomas, P. C. 1994b, Icarus, 107, 18
Drummond, J., Eckart, A., & Hege, E. K. 1988, Icarus, 73, 1
Ďurech, J., Scheirich, P., Kaasalainen, M., et al. 2007, in IAU Symp. 236, eds. G. B. Valsecchi, D. Vokrouhlický, & A. Milani, 191
Ďurech, J., Kaasalainen, M., Warner, B. D., et al. 2009, A&A, 493, 291
Ďurech, J., Sidorin, V., & Kaasalainen, M. 2010, A&A, 513, A46
Ďurech, J., Kaasalainen, M., Herald, D., et al. 2011, Icarus, 214, 652
Durkee, R. I. 2010, Minor Planet Bulletin, 37, 125
Farinella, P., Froeschlé, C., & Gonczi, R. 1994, in Asteroids, Comets, Meteors 1993, eds. A. Milani, M. di Martino, & A. Cellino, IAU Symp., 160, 205
Farinella, P., Vokrouhlický, D., & Hartmann, W. K. 1998, Icarus, 132, 378
Giblin, I., Martelli, G., Farinella, P., et al. 1998, Icarus, 134, 77
Hanuš, J., Ďurech, J., Brož, M., et al. 2011, A&A, 530, A134
Hanuš, J., Ďurech, J., Brož, M., et al. 2013, A&A, 551, A67
Higgins, D. 2011, Minor Planet Bulletin, 38, 41
Higgins, D., & Goncalves, R. M. D. 2007, Minor Planet Bulletin, 34, 16
Johansen, A., & Lacerda, P. 2010, MNRAS, 404, 475
Kaasalainen, M., & Torppa, J. 2001, Icarus, 153, 24
Kaasalainen, M., Torppa, J., & Muinonen, K. 2001, Icarus, 153, 37
Kaasalainen, M., Torppa, J., & Piironen, J. 2002, Icarus, 159, 369
Koff, R. A., Brincat, S. M., Stephens, R. D., & Pravec, P. 2001, Minor Planet Bulletin, 28, 46
Kryszczyńska, A. 2013, A&A, 551, A102
Kryszczyńska, A., La Spina, A., Paolicchi, P., et al. 2007, Icarus, 192, 223
La Spina, A., Paolicchi, P., Kryszczyńska, A., & Pravec, P. 2004, Nature, 428, 400
Lagerkvist, C., Barucci, M. A., Capria, M. T., et al. 1987, Asteroid photometric catalogue (Roma: CNR)
Larson, S., Beshore, E., Hill, R., et al. 2003, in AAS/Division for Planetary Sciences Meeting Abstracts #35, BAAS, 35, 982
Laskar, J., & Robutel, P. 2001, Celest. Mech. Dyn. Astron., 80, 39
Levison, H. F., & Duncan, M. J. 1994, Icarus, 108, 18
Magnusson, P. 1986, Icarus, 68, 1
Marchis, F., Kaasalainen, M., Hom, E. F. Y., et al. 2006, Icarus, 185, 39
Marciniak, A., Michałowski, T., Kaasalainen, M., et al. 2007, A&A, 473, 633
Masiero, J. R., Mainzer, A. K., Grav, T., et al. 2011, ApJ, 741, 68
Michel, P., Jutzi, M., Richardson, D. C., & Benz, W. 2011, Icarus, 211, 535
Nesvorný, D. 2012, in NASA Planetary Data System, 189
Nesvorný, D., & Bottke, W. F. 2004, Icarus, 170, 324
Nesvorný, D., & Morbidelli, A. 1998, AJ, 116, 3029
Nesvorný, D., Jedicke, R., Whiteley, R. J., & Ž. Ivezić. 2005, Icarus, 173, 132
Oey, J. 2006, Minor Planet Bulletin, 33, 96
Paolicchi, P., & Kryszczyńska, A. 2012, Planet. Space Sci., 73, 70
Parker, A., Ž. Ivezić, Jurić, M., et al. 2008, Icarus, 198, 138
Piironen, J., Lagerkvist, C., Torppa, J., Kaasalainen, M., & Warner, B. 2001, BAAS, 33, 1562
Polishook, D., Ofek, E. O., Waszczak, A., et al. 2012, MNRAS, 421, 2094
Pravec, P., Harris, A. W., Kušnirák, P., Galád, A., & Hornoch, K. 2012, Icarus, 221, 365
Pravec, P., Harris, A. W., & Michałowski, T. 2002, Asteroids III, 113
Quinn, T. R., Tremaine, S., & Duncan, M. 1991, AJ, 101, 2287
Rau, A., Kulkarni, S. R., Law, N. M., et al. 2009, PASP, 121, 1334
Rubincam, D. P. 2000, Icarus, 148, 2
Šidlichovský, M., & Nesvorný, D. 1996, Celest. Mech. Dyn. Astron., 65, 137
Skoglöv, E., & Erikson, A. 2002, Icarus, 160, 24
Slivan, S. M. 2002, Nature, 419, 49
Slivan, S. M., & Molnar, L. A. 2012, Icarus, 220, 1097
Slivan, S. M., Binzel, R. P., Crespo da Silva, L. D., et al. 2003, Icarus, 162, 285
Slivan, S. M., Binzel, R. P., Kaasalainen, M., et al. 2009, Icarus, 200, 514
Standish, E. M., Newhall, X. X., Williams, J. G., & Folkner, W. M. 1997, JPL Planetary and Lunar Ephemerides, CD-ROM published by Willmann-Bell, Inc., Richmond, Virginia
Statler, T. S. 2009, Icarus, 202, 502
Stephens, R. D. 2003, Minor Planet Bulletin, 30, 1
Stephens, R. D. 2005, Minor Planet Bulletin, 32, 66
Stephens, R. D. 2007a, Minor Planet Bulletin, 34, 31
Stephens, R. D. 2007b, Minor Planet Bulletin, 34, 102
Stephens, R. D. 2007c, Minor Planet Bulletin, 34, 64
Stephens, R. D. 2011a, Minor Planet Bulletin, 38, 211
Stephens, R. D. 2011b, Minor Planet Bulletin, 38, 23
Strabla, L., Quadri, U., Girelli, R., & Pilcher, F. 2012, Minor Planet Bulletin, 39, 154
Tholen, D. J. 1984, Ph.D. Thesis, Tucson: Arizona Univ.
Tholen, D. J. 1989, in Asteroids II, ed. R. P. Binzel, T. Gehrels, & M. S. Matthews, 1139
Torppa, J., Kaasalainen, M., Michałowski, T., et al. 2003, Icarus, 164, 346
Vokrouhlický, D. 1998, A&A, 335, 1093
Vokrouhlický, D., & Farinella, P. 1998, AJ, 116, 2032
Vokrouhlický, D., & Farinella, P. 1999, AJ, 118, 3049
Vokrouhlický, D., Nesvorný, D., & Bottke, W. F. 2003, Nature, 425, 147
Vokrouhlický, D., Brož, M., Michałowski, T., et al. 2006a, Icarus, 180, 217
Vokrouhlický, D., Nesvorný, D., & Bottke, W. F. 2006b, Icarus, 184, 1
Vokrouhlický, D., Durech, J., Michałowski, T., et al. 2009, A&A, 507, 495
Warner, B. 2001, Minor Planet Bulletin, 28, 40
Warner, B. D. 2004, Minor Planet Bulletin, 31, 19
Warner, B. D. 2005, Minor Planet Bulletin, 32, 29
Warner, B. D. 2006, Minor Planet Bulletin, 33, 82
Warner, B. D. 2009, Minor Planet Bulletin, 36, 172
Warner, B. D. 2010, Minor Planet Bulletin, 37, 112
Warner, B. D. 2011, Minor Planet Bulletin, 38, 63
Warner, B. D., & Pray, D. P. 2009, Minor Planet Bulletin, 36, 166
Warner, B. D., Harris, A. W., & Pravec, P. 2009, Icarus, 202, 134
Zappalà, V., Cellino, A., Farinella, P., & Knežević, Z. 1990, AJ, 100, 2030
Zappalà, V., Cellino, A., Farinella, P., & Milani, A. 1994, AJ, 107, 772

Pages 14 to 19 are available in the electronic edition of the journal at http://www.aanda.org

**Table 3.** Observations not included in the UAPC used for successful model determinations.

| Asteroid | | Date | Observer | Observatory (MPC code) |
|---|---|---|---|---|
| 364 | Isara | 2009 5–2009 05 | Warner (2009) | Palmer Divide Observatory (716) |
| 391 | Ingeborg | 2000 8–2000 12 | Koff et al. (2001) | Antelope Hills Observatory, Bennett (H09) |
| 502 | Sigune | 2007 6 – 2007 6 | Stephens (2007b) | Goat Mountain Astronomical Research Station (G79) |
| 553 | Kundry | 2004 12–2005 1 | Stephens (2005) | Goat Mountain Astronomical Research Station (G79) |
| 616 | Elly | 2010 1–2010 1 | Warner (2010) | Palmer Divide Observatory (716) |
| | | 2010 2–2010 2 | Durkee (2010) | Shed of Science Observatory, USA (H39) |
| 621 | Werdandi | 2012 1 22.9 | Strabla et al. (2012) | Bassano Bresciano Observatory (565) |
| | | 2012 1–2012 2 | Strabla et al. (2012) | Organ Mesa Observatory (G50) |
| 1307 | Chimmeria | 2004 9–2004 9 | Warner (2005) | Palmer Divide Observatory (716) |
| 1396 | Outeniqua | 2006 3–2006 3 | Warner (2006) | Palmer Divide Observatory (716) |
| 1446 | Sillanpaa | 2009 3–2009 3 | Higgins[1] | Hunters Hill Observatory, Ngunnawal (E14) |
| 1464 | Armisticia | 2008 1–2008 1 | Brinsfield (2008b) | Via Capote Sky Observatory, Thousand Oaks (G69) |
| 1619 | Ueta | 2010 9–2010 10 | Higgins (2011) | Hunters Hill Observatory, Ngunnawal (E14) |
| | | 2010 9–2010 9 | Stephens (2011b) | Goat Mountain Astronomical Research Station (G79) |
| 1633 | Chimay | 2008 4–2008 4 | Brinsfield (2008a) | Via Capote Sky Observatory, Thousand Oaks (G69) |
| 1987 | Kaplan | 2000 10–2000 10 | Warner (2001, 2011) | Palmer Divide Observatory (716) |
| | | 2011 12–2011 12 | Warner | Palmer Divide Observatory (716) |
| 2086 | Newell | 2007 1–2007 2 | Stephens (2007c) | Goat Mountain Astronomical Research Station (G79) |
| 2403 | Bruce Helin | 2006 9–2006 9 | Higgins[1] | Hunters Hill Observatory, Ngunnawal (E14) |
| 3279 | Solon | 2006 11–2006 11 | Stephens (2007a) | Goat Mountain Astronomical Research Station (G79) |
| 3492 | Petra-Pepi | 2011 6–2011 7 | Stephens (2011a) | Goat Mountain Astronomical Research Station (G79) |
| 3786 | Yamada | 2002 7–2002 8 | Stephens (2003) | Goat Mountain Astronomical Research Station (G79) |
| 3896 | Pordenone | 2007 10–2007 10 | Higgins[1] | Hunters Hill Observatory, Ngunnawal (E14) |
| 4209 | Briggs | 2003 9–2003 9 | Warner (2004) | Palmer Divide Observatory (716) |
| 4399 | Ashizuri | 2008 6–2008 6 | Brinsfield (2008a) | Via Capote Sky Observatory, Thousand Oaks (G69) |
| 4606 | Saheki | 2009 1–2009 3 | Brinsfield (2009) | Via Capote Sky Observatory, Thousand Oaks (G69) |
| 6159 | 1991 YH | 2006 3–2006 3 | Warner (2006) | Palmer Divide Observatory (716) |
| 6179 | Brett | 2009 4–2009 4 | Warner & Pray (2009) | Palmer Divide Observatory (716) |
| 6262 | Javid | 2010 2–2010 2 | PTF[2] | |
| 6403 | Steverin | 2004 9–2004 9 | Warner (2005) | Palmer Divide Observatory (716) |
| 7043 | Godart | 2008 8–2008 8 | Durkee | Shed of Science Observatory, USA (H39) |
| | | 2008 8–2008 9 | Pravec et al. (2012) | Goat Mountain Astronomical Research Station (G79) |
| 7055 | 1989 KB | 2007 5–2007 5 | Stephens (2007b) | Goat Mountain Astronomical Research Station (G79) |
| | | 2007 5–2007 6 | Higgins[1] | Hunters Hill Observatory, Ngunnawal (E14) |
| 7169 | Linda | 2006 8–2006 8 | Higgins & Goncalves (2007) | Hunters Hill Observatory, Ngunnawal (E14) |
| 7360 | Moberg | 2006 4–2006 4 | Oey (2006) | Leura (E17) |

**Notes.** [(1)] On line at `http://www.david-higgins.com/Astronomy/asteroid/lightcurves.htm` [(2)] Palomar Transient Factory survey (Rau et al. 2009), data taken from Polishook et al. (2012).

**Table 4.** List of asteroids for which the HCM alone suggests membership in families Flora, Koronis, Eos, Eunomia, Phocaea, and Alauda.

| Asteroid | | Status | Reason |
|---|---|---|---|
| | | | Flora |
| 9 | Metis | Interloper | Far from the ($a_p$, $H$) border, peculiar SFD |
| 43 | Ariadne | Interloper | Associated at $v_{\text{cutoff}}$ = 70 m/s, peculiar SFD |
| 352 | Gisela | Borderline | Associated at $v_{\text{cutoff}}$ = 70 m/s, big object |
| 364 | Isara | Interloper | Big, peculiar SFD, close to ($a_p$, $H$) border |
| 376 | Geometria | Interloper | Far from the ($a_p$, $H$) border, peculiar SFD |
| 800 | Kressmannia | Borderline | Associated at $v_{\text{cutoff}}$ = 70 m/s, lower albedo |
| 1188 | Gothlandia | Borderline | Associated at $v_{\text{cutoff}}$ = 70 m/s |
| 1419 | Danzing | Interloper | Far from the ($a_p$, $H$) border |
| 1703 | Barry | Borderline | Associated at $v_{\text{cutoff}}$ = 70 m/s |
| 2839 | Annette | Interloper | Associated at $v_{\text{cutoff}}$ = 70 m/s, C type |
| 7360 | Moberg | Borderline | Redder (color from SDSS MOC4) |
| | | | Koronis |
| 167 | Urda | Borderline | Close to the ($a_p$, $H$) border |
| 208 | Lacrimosa | Interloper | Far from the ($a_p$, $H$) border, peculiar SFD |
| 311 | Claudia | Borderline | Close to the ($a_p$, $H$) border |
| 720 | Bohlinia | Borderline | Close to the ($a_p$, $H$) border |
| 1835 | Gajdariya | Interloper | Close to the ($a_p$, $H$) border, incompatible albedo |
| 2953 | Vysheslavia | Borderline | Close to the ($a_p$, $H$) border |
| 3170 | Dzhanibekov | Interloper | Behind the ($a_p$, $H$) border, incompatible albedo |
| | | | Eos |
| 423 | Diotima | Interloper | Far from the ($a_p$, $H$) border, big, C type |
| 590 | Tomyris | Borderline | Close to the ($a_p$, $H$) border |
| | | | Eunomia |
| 85 | Io | Interloper | Behind the ($a_p$, $H$) border, peculiar SFD, incompatible albedo |
| 390 | Alma | Borderline | Borderline albedo, borderline in ($a_p$, $e_p$, $I_p$) space |
| 4399 | Ashizuri | Borderline | Close to the ($a_p$, $H$) border |
| | | | Phocaea |
| 290 | Bruna | Borderline | Close to the ($a_p$, $H$) border |
| 391 | Ingeborg | Interloper | Clearly outside ($a_p$, $H$) |
| 852 | Wladilena | Borderline | Slightly outside ($a_p$, $H$) |
| 1963 | Bezovec | Interloper | C type, incompatible albedo ($p_V$ = 0.04) |
| 5647 | 1990 TZ | Interloper | Incompatible albedo ($p_V$ = 0.64) |
| | | | Themis |
| 62 | Erato | Borderline | Close to the ($a_p$, $H$) border |
| 1633 | Chimay | Borderline | Close to the ($a_p$, $H$) border |
| | | | Maria |
| 695 | Bella | Borderline | Close to the ($a_p$, $H$) border |
| 714 | Ulula | Borderline | Close to the ($a_p$, $H$) border |
| | | | Alauda |
| 276 | Adelheid | Interloper | Far from the ($a_p$, $H$) border, big |

**Notes.** By additional methods for determining family membership we identify them as interlopers or borderline cases. We also give the name of the asteroid, the family membership according the HCM, if it is an interloper or a borderline case and the reason. Peculiar SFD means a size frequency distribution that is incompatible with the SFD typically created by catastrophic collisions or cratering events (i.e., a large remnant, large fragment, and steep slope). Quantity $v_{\text{cutoff}}$ corresponds to the cutoff value of the HCM for a particular family.

**Table 5.** List of asteroids that (i) have been identified as members of the Flora, Koronis, Eos, Eunomia, Phocaea, Themis, Maria, Vesta, Nysa/Polana, and Alauda families by the HCM; and (ii) for which shape models from LI are available in the DAMIT database or are newly derived.

| Asteroid | $\lambda_1$ [deg] | $\beta_1$ [deg] | $\lambda_2$ [deg] | $\beta_2$ [deg] | $P$ [hours] | $a_p$ [AU] | $D$ [km] | Bus/DeMeo | Tholen | $p_V$ | M/I/B | Reference |
|---|---|---|---|---|---|---|---|---|---|---|---|---|
| | | | | | | | Flora | | | | | |
| 8 Flora | 335 | −5 | 155 | 6 | 12.8667 | 2.2014 | 141.0 | – | S | 0.26 ± 0.05 | M | Torppa et al. (2003) |
| 9 Metis | 180 | 22 | | | 5.079177 | 2.3864 | 169.0 | – | S | 0.13 ± 0.02 | I | Torppa et al. (2003) |
| 43 Ariadne | 253 | −15 | | | 5.761987 | 2.2034 | 72.1 | Sk | S | 0.23 ± 0.05 | I | Kaasalainen et al. (2002) |
| 281 Lucretia | 128 | −49 | 309 | −61 | 4.349711 | 2.1878 | 11.8 | S | SU | 0.20 ± 0.01 | M | Hanuš et al. (2013)/Kryszczyńska (2013) |
| 352 Gisela | 205 | −26 | 23 | −20 | 7.48008 | 2.1941 | 26.7 | Sl | S | 0.19 ± 0.02 | B | Hanuš et al. (2013) |
| 364 Isara | 282 | 44 | 86 | 42 | 9.15748 | 2.2208 | 35.2 | – | S | 0.16 ± 0.03 | I | this work |
| 376 Geometria | 239 | 45 | 63 | 53 | 7.71098 | 2.2886 | 39.0 | Sl | S | 0.19 ± 0.04 | I | Hanuš et al. (2011) |
| 540 Rosamunde | 301 | 81 | 127 | 62 | 9.34779 | 2.2189 | 20.3 | – | S | 0.22 ± 0.05 | M | this work |
| 553 Kundry | 197 | 73 | 359 | 64 | 12.6025 | 2.2308 | 9.6 | S | – | 0.25 ± 0.04 | M | this work |
| 685 Hermia | 197 | 87 | 29 | 79 | 50.387 | 2.2359 | 10.9 | – | – | 0.28 ± 0.05 | M | Hanuš et al. (2011) |
| 700 Auravictrix | 67 | 46 | 267 | 51 | 6.074836 | 2.2295 | 20.6 | – | – | 0.14 ± 0.05 | M | Kryszczyńska (2013) |
| 800 Kressmannia | 345 | 37 | 172 | 34 | 4.460964 | 2.1927 | 17.0 | – | S | 0.15 ± 0.02 | B | Hanuš et al. (2011) |
| 823 Sisigambis | 86 | 74 | | | 146.58 | 2.2213 | 15.8 | – | – | 0.23 ± 0.03 | M | Hanuš et al. (2011) |
| 915 Cosette | 350 | 56 | 189 | 61 | 4.46974 | 2.2277 | 12.3 | – | – | 0.23 ± 0.04 | M | Ďurech et al. (2009) |
| 951 Gaspra | 20 | 23 | 198 | 15 | 7.04203 | 2.2097 | 12.2 | S | S | 0.33 ± 0.13 | M | this work |
| | 19 | 21 | | | | | | | | | | Davies et al. (1994b)[1] |
| 1056 Azalea | 242 | 61 | 49 | 48 | 15.0276 | 2.2300 | 13.0 | S | – | 0.25 ± 0.04 | M | Hanuš et al. (2013) |
| 1088 Mitaka | 280 | −71 | | | 3.035378 | 2.2014 | 16.0 | S | S | 0.16 ± 0.02 | M | Hanuš et al. (2011) |
| 1185 Nikko | 359 | 34 | | | 3.786149 | 2.2375 | 11.3 | S | S | 0.20 | M | Hanuš et al. (2011)/Ďurech et al. (2009) |
| 1188 Gothlandia | 133 | −84 | 335 | −81 | 3.491820 | 2.1907 | 12.7 | S | – | 0.25 ± 0.02 | B | Hanuš et al. (2013)/Kryszczyńska (2013) |
| 1249 Rutherfordia | 204 | 72 | 31 | 74 | 18.2183 | 2.2243 | 14.1 | – | S | 0.22 ± 0.02 | M | Hanuš et al. (2013) |
| 1270 Datura | 60 | 76 | | | 3.358100 | 2.2347 | 8.2 | – | – | 0.24 | M | Vokrouhlický et al. (2009) |
| 1307 Cimmeria | | 63 | | | 2.820723 | 2.2505 | 10.1 | – | S | 0.22 ± 0.02 | B | this work |
| 1396 Outeniqua | | 62 | | | 3.08175 | 2.2480 | 11.7 | – | – | 0.21 ± 0.01 | M | this work |
| 1419 Danzig | 22 | 76 | 193 | 62 | 8.11957 | 2.2928 | 14.1 | – | – | 0.24 ± 0.05 | I | Hanuš et al. (2011) |
| 1446 Sillanpaa | 129 | 76 | 288 | 63 | 9.65855 | 2.2457 | 8.8 | – | – | 0.21 ± 0.01 | M | this work |
| 1514 Ricouxa | 251 | 75 | 68 | 69 | 10.42467 | 2.2404 | 8.1 | – | – | 0.18 ± 0.04 | M | Hanuš et al. (2011) |
| 1518 Rovaniemi | 62 | 60 | 265 | 45 | 5.25047 | 2.2255 | 9.0 | – | – | 0.26 ± 0.04 | M | Hanuš et al. (2013) |
| 1527 Malmquista | 274 | 80 | | | 14.0591 | 2.2274 | 10.3 | – | – | 0.22 ± 0.02 | M | this work |
| 1619 Ueta | | 39 | | | 2.717943 | 2.2411 | 9.9 | – | S | 0.25 ± 0.03 | M | this work |
| 1675 Simonida | 23 | 58 | 227 | 54 | 5.287962 | 2.2332 | 11.1 | – | – | 0.25 ± 0.03 | M | Kryszczyńska (2013) |
| 1682 Karel | 232 | 32 | 51 | 41 | 3.37486 | 2.2388 | 7.1 | – | – | 0.24 | M | Hanuš et al. (2011) |
| 1703 Barry | 46 | −76 | 221 | −71 | 107.04 | 2.2148 | 9.4 | – | – | 0.22 ± 0.03 | B | this work |
| 1738 Oosterhoff | | −72 | | | 4.44896 | 2.1835 | 8.7 | S | – | 0.28 ± 0.04 | M | this work |
| 1785 Wurm | 11 | 57 | 192 | 47 | 3.26934 | 2.2359 | 6.2 | S | – | 0.24 | M | Hanuš et al. (2013) |
| 2017 Wesson | 159 | 81 | 356 | 79 | 3.415579 | 2.2521 | 7.2 | – | – | 0.20 ± 0.05 | M | Kryszczyńska (2013) |
| 2094 Magnitka | 107 | 57 | 272 | 48 | 6.11219 | 2.2323 | 12.1 | – | – | 0.13 ± 0.01 | M | Hanuš et al. (2013) |
| 2112 Ulyanov | 151 | 61 | 331 | 61 | 3.04071 | 2.2547 | 7.5 | – | – | 0.24 | M | Hanuš et al. (2013) |
| 2510 Shandong | 256 | 27 | 71 | 27 | 5.94638 | 2.2531 | 9.0 | – | S | 0.20 | M | Hanuš et al. (2013) |
| 2709 Sagan | 308 | −8 | 124 | −16 | 5.25638 | 2.1954 | 6.8 | S | – | 0.24 | M | Hanuš et al. (2013) |
| 2839 Annette | 341 | −49 | 154 | −36 | 10.4609 | 2.2166 | 7.6 | – | – | 0.06 ± 0.01 | I | Hanuš et al. (2013) |

**Notes.** For each asteroid, the table gives the spin state solution (i.e., ecliptic coordinates $\lambda$ and $\beta$ of the spin axis and the sidereal rotational period $P$, usually for both ambiguous pole solutions), the proper semi-major axis $a_p$, the diameter $D$ and albedo $p_v$ based on WISE data (Masiero et al. 2011), the SMASS II taxonomy (Bus & Binzel 2002), the Tholen (Tholen 1984, 1989) taxonomical type, the information if the asteroid is, according to our membership revision, a member (M), an interloper (I) or a borderline case (B), and the reference to the convex model. [(1)] The spin vector solution of asteroid (951) Gaspra is based on Galileo images obtained during the October 1991 flyby. [(2)] The solution of asteroid (243) Ida is based on Galileo images and photometric data.

**Table 5.** continued.

| Asteroid | $\lambda_1$ [deg] | $\beta_1$ [deg] | $\lambda_2$ [deg] | $\beta_2$ [deg] | $P$ [hours] | $a_p$ [AU] | $D$ [km] | Bus/DeMeo | Tholen | $p_V$ | M/I/B | Reference |
|---|---|---|---|---|---|---|---|---|---|---|---|---|
| 3279 Solon | 268 | −70 | | | 8.1041 | 2.2027 | 5.9 | – | – | 0.24 | M | this work |
| 7043 Godart | 73 | 62 | 235 | 80 | 8.4518 | 2.2447 | 5.7 | – | – | 0.23 ± 0.04 | M | this work |
| 7169 Linda | 11 | −60 | 198 | −61 | 27.864 | 2.2487 | 4.5 | – | – | 0.24 | M | this work |
| 7360 Moberg | | −18 | | | 4.58533 | 2.2510 | 7.7 | – | – | 0.22 ± 0.04 | B | this work |
| | | | | | | | Flora | | | | | |
| 31383 1998 XJ$_9$4 | 110 | −74 | 279 | −63 | 4.16818 | 2.1853 | 4.1 | – | – | 0.29 ± 0.03 | M | Hanuš et al. (2013) |
| | | | | | | | Koronis | | | | | |
| 158 Koronis | 30 | −64 | | | 14.2057 | 2.8687 | 47.7 | S | S | 0.14 ± 0.01 | M | Ďurech et al. (2011) |
| | 220 | −68 | 35 | −65 | 14.20569 | | | | | | | Slivan et al. (2003) |
| 167 Urda | 249 | −68 | 107 | −69 | 13.06133 | 2.8535 | 44.0 | Sk | S | 0.16 ± 0.04 | B | Ďurech et al. (2011) |
| | 225 | −73 | 40 | −75 | 13.06135 | | | | | | | Slivan et al. (2003) |
| 208 Lacrimosa | 170 | −68 | 350 | −71 | 14.076919 | 2.8929 | 45.0 | Sk | S | 0.17 ± 0.06 | I | Slivan et al. (2003) |
| 243 Ida | 259 | −66 | 74 | −61 | 4.633632 | 2.8616 | 28.0 | S | S | 0.24 ± 0.07 | M | this work |
| | 263 | −67 | | | 4.633632 | | | | | | | Davies et al. (1994a); Binzel et al. (1993)[2] |
| 263 Dresda | 105 | 76 | 285 | 80 | 16.81387 | 2.8865 | 25.5 | S | – | 0.18 ± 0.02 | M | Slivan et al. (2009) |
| 277 Elvira | 121 | −84 | | | 29.69219 | 2.8856 | 31.2 | – | S | 0.20 ± 0.05 | M | Hanuš et al. (2011) |
| | 50 | −80 | 244 | −81 | 29.69218 | | | | | | | Slivan et al. (2009) |
| 311 Claudia | 214 | 43 | 30 | 40 | 7.5314 | 2.8976 | 25.8 | – | S | 0.24 ± 0.03 | B | Hanuš et al. (2011) |
| | 209 | 48 | 24 | 48 | 7.53139 | | | | | | | Slivan et al. (2003) |
| 321 Florentina | 264 | −63 | 91 | −60 | 2.870866 | 2.8856 | 34.0 | S | S | 0.14 ± 0.01 | M | Slivan et al. (2003) |
| 462 Eriphyla | 108 | 35 | 294 | 34 | 8.65890 | 2.8737 | 41.9 | S | S | 0.17 ± 0.02 | M | Slivan et al. (2009) |
| 534 Nassovia | 66 | 41 | 252 | 42 | 9.46889 | 2.8842 | 38.6 | Sq | S | 0.12 ± 0.02 | M | Hanuš et al. (2011) |
| | 58 | 50 | 244 | 50 | 9.46896 | | | | | | | Slivan et al. (2003) |
| 720 Bohlinia | 230 | 41 | 40 | 43 | 8.91862 | 2.8873 | 34.0 | Sq | S | 0.20 ± 0.02 | B | Slivan et al. (2003) |
| 832 Karin | 242 | 46 | 59 | 44 | 18.35123 | 2.8644 | 16.3 | – | – | 0.21 ± 0.05 | M | Hanuš et al. (2011) |
| | 230 | 42 | 52 | 42 | 18.352 | | | | | | | Slivan & Molnar (2012) |
| 1223 Neckar | 252 | 28 | 69 | 30 | 7.82401 | 2.8695 | 25.7 | – | S | 0.15 ± 0.03 | M | Hanuš et al. (2011) |
| | 259 | 41 | 73 | 40 | 7.82124 | | | | | | | Slivan et al. (2003) |
| 1289 Kutaissi | 158 | −79 | 338 | −74 | 3.624174 | 2.8605 | 22.6 | – | S | 0.16 ± 0.04 | M | Slivan et al. (2003) |
| 1350 Rosselia | 166 | −72 | | | 8.14011 | 2.8580 | 21.1 | Sa | S | 0.20 ± 0.05 | M | Hanuš et al. (2011) |
| 1389 Onnie | 183 | −75 | 360 | −79 | 23.0447 | 2.8661 | 14.7 | – | – | 0.17 ± 0.04 | M | Hanuš et al. (2013) |
| 1423 Jose | 78 | −82 | | | 12.3127 | 2.8602 | 20.0 | S | – | 0.28 ± 0.04 | M | this work |
| 1482 Sebastiana | 262 | −68 | 91 | −67 | 10.48966 | 2.8723 | 17.6 | – | – | 0.21 ± 0.05 | M | Hanuš et al. (2011) |
| 1618 Dawn | 39 | −60 | 215 | −51 | 43.219 | 2.8688 | 17.5 | S | – | 0.15 ± 0.04 | M | this work |
| 1635 Bohrmann | 5 | −38 | 185 | −36 | 5.86427 | 2.8534 | 17.5 | S | – | 0.21 ± 0.02 | M | Hanuš et al. (2011) |
| 1742 Schaifers | 56 | 52 | 247 | 68 | 8.53271 | 2.8892 | 16.6 | – | – | 0.11 ± 0.02 | M | Hanuš et al. (2011) |
| 1835 Gajdariya | 34 | 74 | 204 | 69 | 6.33768 | 2.8331 | 12.8 | – | – | 0.27 ± 0.04 | I | this work |
| 2953 Vysheslavia | 11 | −64 | 192 | −68 | 6.29453 | 2.8282 | 12.8 | S | – | 0.25 ± 0.07 | B | Vokrouhlický et al. (2006a) |
| 3170 Dzhanibekov | 216 | 62 | 30 | 63 | 6.07167 | 2.9291 | 9.6 | S | – | 0.30 ± 0.04 | I | Hanuš et al. (2013) |
| 4507 1990 FV | 137 | 50 | 307 | 51 | 6.57932 | 2.8689 | 11.0 | – | – | 0.28 ± 0.02 | M | Hanuš et al. (2013) |
| 6262 Javid | 93 | 76 | 275 | 69 | 8.02054 | 2.9063 | 7.8 | – | – | 0.29 ± 0.04 | M | this work |
| | | | | | | | Eos | | | | | |
| 423 Diotima | 351 | 4 | | | 4.775377 | 3.0684 | 177.3 | C | C | 0.07 ± 0.00 | I | Marchis et al. (2006) |
| 573 Recha | 74 | −24 | 252 | −48 | 7.16585 | 3.0138 | 44.4 | – | – | 0.13 ± 0.02 | M | Hanuš et al. (2011) |
| 590 Tomyris | 273 | −47 | 120 | −46 | 5.55247 | 3.0006 | 31.1 | – | – | 0.18 ± 0.03 | B | Hanuš et al. (2011) |
| 669 Kypria | 31 | 40 | 190 | 50 | 14.2789 | 3.0114 | 29.2 | – | S | 0.17 ± 0.02 | M | Hanuš et al. (2013) |
| 807 Ceraskia | 325 | 23 | 132 | 26 | 7.37390 | 3.0185 | 21.4 | – | S | 0.21 ± 0.05 | M | Hanuš et al. (2013) |

**Table 5.** continued.

| Asteroid | $\lambda_1$ [deg] | $\beta_1$ [deg] | $\lambda_2$ [deg] | $\beta_2$ [deg] | $P$ [hours] | $a_p$ [AU] | $D$ [km] | Bus/DeMeo | Tholen | $p_V$ | M/I/B | Reference |
|---|---|---|---|---|---|---|---|---|---|---|---|---|
| 1087 Arabis | 334 | −7 | 155 | 12 | 5.79499 | 3.0150 | 45.6 | – | S | $0.10 \pm 0.01$ | M | Hanuš et al. (2011) |
| 1148 Rarahu | 148 | −9 | 322 | −9 | 6.54448 | 3.0161 | 26.3 | K | S | $0.22 \pm 0.06$ | M | Hanuš et al. (2011) |
| 1207 Ostenia | 310 | −77 | 124 | −51 | 9.07129 | 3.0207 | 22.9 | – | – | $0.13 \pm 0.02$ | M | Hanuš et al. (2011) |
| 1286 Banachiewicza | 214 | 62 | 64 | 60 | 8.63041 | 3.0223 | 22.6 | – | S | $0.16 \pm 0.03$ | M | this work |
| 1291 Phryne | 106 | 35 | 277 | 59 | 5.58414 | 3.0130 | 22.4 | – | – | $0.19 \pm 0.04$ | M | Hanuš et al. (2011) |
| 1339 Desagneauxa | | 65 | | | 9.37510 | 3.0211 | 26.1 | – | S | $0.12 \pm 0.02$ | M | this work |
| 1353 Maartje | 266 | 73 | 92 | 57 | 22.9927 | 3.0120 | 42.2 | – | – | $0.07 \pm 0.00$ | M | this work |
| 1464 Armisticia | 194 | −54 | 35 | −69 | 7.46699 | 3.0035 | 23.3 | – | – | $0.13 \pm 0.36$ | M | this work |
| 2957 Tatsuo | 88 | 57 | 246 | 37 | 6.82042 | 3.0221 | 22.9 | K | – | $0.29 \pm 0.02$ | M | Hanuš et al. (2013) |
| 3896 Pordenone | | −32 | | | 4.00366 | 3.0057 | 20.0 | – | – | $0.13 \pm 0.01$ | M | this work |
| 5281 Lindstrom | 238 | −72 | 84 | −81 | 9.2511 | 3.0125 | 20.0 | – | – | | M | Hanuš et al. (2013) |
| 19848 Yeungchuchiu | 66 | −70 | 190 | −67 | 3.45103 | 3.0075 | 13.2 | – | – | $0.21 \pm 0.03$ | M | Hanuš et al. (2013) |
| | | | | | | | Eunomia | | | | | |
| 15 Eunomia | 363 | −67 | | | 6.082752 | 2.6437 | 259.0 | S | S | $0.21 \pm 0.06$ | M | Kaasalainen et al. (2002) |
| 85 Io | 95 | −65 | | | 6.87478 | 2.6537 | 161.0 | B | FC | $0.06 \pm 0.03$ | I | Ďurech et al. (2011) |
| 390 Alma | 54 | −48 | 263 | −73 | 3.74117 | 2.6517 | 31.2 | – | DT | $0.13 \pm 0.02$ | B | Hanuš et al. (2013) |
| 812 Adele | 301 | 44 | 154 | 69 | 5.85745 | 2.6594 | 13.6 | – | – | $0.24 \pm 0.03$ | M | Hanuš et al. (2013) |
| 1333 Cevenola | 8 | −79 | 201 | −40 | 4.87933 | 2.6336 | 17.1 | – | – | $0.17 \pm 0.04$ | M | Hanuš et al. (2011) |
| 1495 Helsinki | 356 | −33 | | | 5.33131 | 2.6392 | 13.3 | – | – | $0.23 \pm 0.02$ | M | Hanuš et al. (2013) |
| 1503 Kuopio | 170 | −86 | 27 | −61 | 9.9586 | 2.6263 | 18.4 | – | – | $0.30 \pm 0.06$ | M | this work |
| 1554 Yugoslavia | 281 | −34 | 78 | −64 | 3.88766 | 2.6194 | 17.2 | – | – | $0.10 \pm 0.01$ | M | Hanuš et al. (2013) |
| 1927 Suvanto | 90 | 39 | 277 | 6 | 8.16154 | 2.6497 | 12.5 | – | – | $0.26 \pm 0.04$ | M | Hanuš et al. (2013) |
| 2384 Schulhof | 194 | −57 | 46 | −36 | 3.29367 | 2.6099 | 11.7 | – | – | $0.27 \pm 0.02$ | M | Hanuš et al. (2013) |
| 3017 Petrovic | | −73 | | | 4.08037 | 2.6074 | 12.7 | – | – | $0.21 \pm 0.02$ | M | this work |
| 3492 Petra−Pepi | 9 | −57 | 202 | −16 | 46.570 | 2.6159 | 12.2 | – | – | $0.23 \pm 0.03$ | M | this work |
| 4399 Ashizuri | 266 | −48 | 45 | −61 | 2.830302 | 2.5759 | 8.8 | – | – | $0.28 \pm 0.06$ | B | this work |
| 4467 Kaidanovskij | | 54 | | | 19.1454 | 2.6383 | 11.6 | – | – | 0.21 | M | this work |
| 8132 Vitginzburg | 33 | −66 | 193 | −48 | 7.27529 | 2.6263 | 11.6 | – | – | 0.21 | M | Hanuš et al. (2013) |
| | | | | | | | Phocaea | | | | | |
| 25 Phocaea | 347 | 10 | | | 9.935397 | 2.4002 | 75.1 | S | S | $0.23 \pm 0.02$ | M | Hanuš et al. (2013) |
| 290 Bruna | 286 | −80 | 37 | −74 | 13.8055 | 2.3372 | 10.4 | – | – | $0.42 \pm 0.08$ | B | Hanuš et al. (2013) |
| 391 Ingeborg | | −60 | | | 26.4145 | 2.3202 | 19.6 | S | S | 0.20 | I | this work |
| 502 Sigune | | −44 | | | 10.92667 | 2.3831 | 19.5 | – | S | $0.23 \pm 0.02$ | M | this work |
| 852 Wladilena | 218 | −41 | 57 | −16 | 4.613301 | 2.3627 | 31.1 | – | – | $0.16 \pm 0.02$ | B | Hanuš et al. (2013) |
| 1192 Prisma | | −65 | | | 6.55836 | 2.3660 | 7.2 | – | – | 0.23 | M | this work |
| 1568 Aisleen | 109 | −68 | | | 6.67598 | 2.3520 | 12.0 | – | – | $0.18 \pm 0.03$ | M | Hanuš et al. (2011) |
| 1963 Bezovec | 218 | 16 | 50 | −49 | 18.1655 | 2.4231 | 45.0 | – | C | $0.04 \pm 0.01$ | I | Hanuš et al. (2013) |
| 1987 Kaplan | 357 | −58 | | | 9.45950 | 2.3822 | 14.6 | – | – | $0.21 \pm 0.04$ | M | this work |
| 2430 Bruce Helin | 177 | −68 | | | 129.75 | 2.3627 | 12.7 | Sl | S | 0.23 | M | this work |
| 5647 1990 TZ | 266 | 69 | | | 6.13868 | 2.4241 | 9.3 | S | – | $0.64 \pm 0.07$ | I | Hanuš et al. (2013) |
| 6179 Brett | | −42 | | | 9.4063 | 2.4278 | 5.8 | – | – | 0.23 | M | this work |
| 7055 1989 KB | | −61 | | | 4.16878 | 2.3496 | 6.7 | – | – | $0.33 \pm 0.15$ | M | this work |
| 10772 1990 YM | 16 | 46 | | | 68.82 | 2.3901 | 6.2 | – | – | $0.38 \pm 0.06$ | M | Hanuš et al. (2013) |
| | | | | | | | Themis | | | | | |
| 62 Erato | 87 | 22 | 269 | 23 | 9.21813 | 3.1217 | 95.4 | Ch | BU | $0.06 \pm 0.00$ | B | Hanuš et al. (2011) |
| 222 Lucia | 107 | 54 | 290 | 51 | 7.83671 | 3.1349 | 56.5 | – | BU | $0.12 \pm 0.02$ | M | Hanuš et al. (2013) |
| 621 Werdandi | 247 | −86 | 66 | −77 | 11.77456 | 3.1193 | 27.1 | – | FCX | $0.15 \pm 0.02$ | M | this work |
| 936 Kunigunde | 47 | 57 | 234 | 50 | 8.82653 | 3.1383 | 39.6 | – | – | $0.11 \pm 0.01$ | M | this work |

**Table 5.** continued.

| Asteroid | $\lambda_1$ [deg] | $\beta_1$ [deg] | $\lambda_2$ [deg] | $\beta_2$ [deg] | $P$ [hours] | $a_p$ [AU] | $D$ [km] | Bus/DeMeo | Tholen | $p_V$ | M/I/B | Reference |
|---|---|---|---|---|---|---|---|---|---|---|---|---|
| 1003 Lilofee | | 65 | | | 8.24991 | 3.1483 | 31.4 | – | – | $0.15 \pm 0.04$ | M | this work |
| 1623 Vivian | | −75 | | | 20.5235 | 3.1347 | 29.6 | – | – | 0.08 | M | this work |
| 1633 Chimay | 322 | 77 | 116 | 81 | 6.59064 | 3.1748 | 37.7 | – | – | $0.08 \pm 0.01$ | B | this work |
| 1691 Oort | 45 | 68 | 223 | 58 | 10.2684 | 3.1664 | 33.2 | – | CU | $0.07 \pm 0.01$ | M | this work |
| 1805 Dirikis | 364 | 48 | 188 | 61 | 23.4543 | 3.1333 | 28.1 | – | – | $0.09 \pm 0.01$ | M | this work |
| | | | | | | | Maria | | | | | |
| 616 Elly | | 67 | | | 5.29771 | 2.5526 | 22.6 | – | S | $0.19 \pm 0.04$ | M | this work |
| 695 Bella | 87 | −55 | 314 | −56 | 14.21899 | 2.5391 | 41.2 | – | S | $0.24 \pm 0.03$ | B | Hanuš et al. (2011) |
| 714 Ulula | 224 | −10 | 41 | −5 | 6.99838 | 2.5352 | 39.2 | – | S | $0.27 \pm 0.04$ | B | Hanuš et al. (2011) |
| 787 Moskva | 330 | 60 | 122 | 19 | 6.05581 | 2.5396 | 40.3 | – | – | $0.12 \pm 0.02$ | M | Hanuš et al. (2013) |
| 875 Nymphe | 42 | 31 | 196 | 42 | 12.6213 | 2.5539 | 15.2 | – | – | $0.19 \pm 0.02$ | M | Hanuš et al. (2013) |
| 1160 Illyria | | 47 | | | 4.10295 | 2.5604 | 14.8 | – | – | $0.22 \pm 0.04$ | M | this work |
| 1996 Adams | 107 | 55 | | | 3.31114 | 2.5587 | 13.5 | – | – | $0.14 \pm 0.01$ | M | Hanuš et al. (2013) |
| 3786 Yamada | | 56 | | | 4.03294 | 2.5503 | 16.7 | – | – | $0.23 \pm 0.04$ | M | this work |
| 6403 Steverin | 246 | 77 | 109 | 73 | 3.49119 | 2.5945 | 6.9 | – | – | $0.49 \pm 0.05$ | M | this work |
| | | | | | | | Vesta | | | | | |
| 63 Ausonia | 305 | −21 | 120 | −15 | 9.29759 | 2.3952 | 90.0 | Sa | S | $0.16 \pm 0.03$ | – | Torppa et al. (2003) |
| 306 Unitas | 79 | −35 | | | 8.73874 | 2.3580 | 49.0 | S | S | $0.17 \pm 0.06$ | – | Ďurech et al. (2007) |
| 336 Lacadiera | 194 | 39 | 37 | 54 | 13.69555 | 2.2518 | 69.0 | Xk | D | $0.05 \pm 0.01$ | – | Hanuš et al. (2011) |
| 556 Phyllis | 34 | 54 | 209 | 41 | 4.292622 | 2.4654 | 38.5 | S | S | $0.18 \pm 0.03$ | – | Marciniak et al. (2007) |
| 1933 Tinchen | 113 | 26 | 309 | 36 | 3.67062 | 2.3530 | 6.5 | – | – | $0.29 \pm 0.06$ | – | Hanuš et al. (2013) |
| 2086 Newell | | −60 | | | 78.09 | 2.4014 | 9.8 | Xc | – | 0.20 | – | this work |
| 6159 1991 YH | 266 | 67 | 62 | 67 | 10.6589 | 2.2914 | 5.4 | – | – | $0.46 \pm 0.13$ | – | this work |
| 8359 1989 WD | 121 | −68 | 274 | −68 | 2.89103 | 2.3500 | 8.2 | – | – | $0.22 \pm 0.03$ | – | Hanuš et al. (2013) |
| | | | | | | | Nysa/Polana | | | | | |
| 44 Nysa | 99 | 58 | | | 6.421417 | 2.4227 | 70.6 | Xc | E | $0.55 \pm 0.07$ | – | Kaasalainen et al. (2002) |
| 135 Hertha | 272 | 52 | | | 8.40060 | 2.4285 | 77.0 | Xk | M | $0.15 \pm 0.05$ | – | Torppa et al. (2003) |
| 1378 Leonce | 210 | −67 | 46 | −77 | 4.32526 | 2.3748 | 22.5 | – | – | $0.03 \pm 0.00$ | – | this work |
| 1493 Sigrid | | 78 | | | 43.179 | 2.4297 | 22.1 | Xc | F | $0.04 \pm 0.00$ | – | this work |
| 4606 Saheki | 44 | 59 | 222 | 68 | 4.97347 | 2.2518 | 6.7 | – | – | $0.33 \pm 0.02$ | – | this work |
| | | | | | | | Alauda | | | | | |
| 276 Adelheid | 199 | −20 | 9 | −4 | 6.319200 | 3.1162 | 125.0 | – | X | $0.06 \pm 0.01$ | I | Marciniak et al. (2007) |
| 1276 Ucclia | | −49 | | | 4.90748 | 3.1698 | 40.0 | – | – | $0.05 \pm 0.01$ | M | this work |
| 1838 Ursa | | 47 | | | 16.1635 | 3.2111 | 48.6 | – | – | $0.04 \pm 0.01$ | M | this work |
| 4209 Briggs | | −56 | | | 12.2530 | 3.1564 | 30.9 | – | – | $0.09 \pm 0.03$ | M | this work |